Journal of Geochemical Exploration 165 (2016) 143–158

Contents lists available at ScienceDirect

Journal of Geochemical Exploration

journal homepage: www.elsevier.com/locate/gexplo

Recognizing and quantifying metamorphosed alteration zones through amphibolite facies metamorphic overprint at the Key Anacon Zn–Pb–Cu–Ag deposits, Bathurst Mining Camp, New Brunswick, Canada

Joseph D.S. Zulu [a,*], David R. Lentz [a], James A. Walker [b], Christopher R.M. McFarlane [a]

[a] Department of Earth Sciences, University of New Brunswick, Fredericton, New Brunswick E3B 5A3, Canada
[b] Geological Surveys Branch, New Brunswick Department of Energy and Mines, P.O. Box 50, Bathurst, New Brunswick E2A 3Z1, Canada

ARTICLE INFO

Article history:
Received 29 December 2014
Revised 25 January 2016
Accepted 16 February 2016
Available online 23 February 2016

Keywords:
Hydrothermal alteration
Compositional change
Key Anacon
Sulfidation and oxidation

ABSTRACT

The Key Anacon deposits, Bathurst Mining Camp, New Brunswick, are hosted in upper greenschist- to amphibolite-facies felsic volcanic rocks. The occurrence of cordierite–biotite and garnet–biotite–muscovite assemblages parallel to the regional tectonic fabric in the metamorphosed hydrothermal alteration zones point to a pre-metamorphic mineralization event that was synchronous with sub-aqueous volcanism. Modeling the altered felsic volcanic rocks in the system K_2O–Fe_2O_3–MgO–Al_2O_3–SiO_2–H_2O–TiO_2 (KFMASHT) and comparing the observed peak metamorphic assemblages with those produced in a petrogenetic grid allows us to interpret the style of pre-metamorphic hydrothermal alteration related to deposit formation. The compositional change in the stratigraphic footwall (structural hanging wall) is characterized by mass gains of 0.1 to 4.0 wt.% $Fe_2O_{3\ (Total)}$, 0.7 to 22.2 wt.% MgO, and 0.5 to 55.2 wt.% CaO, and mass losses of 25.1 to 56.7 wt.% SiO_2, 0.2 to 2.0 wt.% Na_2O, and 0.3 to 3.8 wt.% K_2O (the values of the mass changes cited here are in absolute terms).Variable gains and losses of Zn, Pb, and Cu are characteristic of the footwall alteration zones with Zn displaying gains proximal to the massive sulfide lens, and losses distal to the sulfide lens. The alteration indices (AI) values increase as the massive sulfide lens are approached from either the footwall or hanging wall, whereas the Ghandi index (GI) discriminates the intensely chlorite-altered rocks proximal to mineralization from the sericitic altered rock in more distal areas. Overall, there is an increase of the GI from the weakly to moderately altered zone (GI = 1.3 to 6.0) to the more intensely altered zone (GI = 6.1 to 60). These physical and geochemical observations are consistent with early feldspar-destructive alteration followed by chloritization proximal to the sulfide lens and accompanied by sericitization alteration distal prior to sulfidation and oxidation during prograde metamorphism.

1. Introduction

The processes and hydrothermal fluids that form volcanogenic massive sulfide (VMS) deposits are the same processes and fluids that give rise to alteration assemblages. Understanding the alteration processes has an economic significance in that it allows the geologist to use it as a vector towards an ore deposit. As mineralizing fluids migrate through the footwall stratigraphy some elements move from the host rocks into the fluid, whereas other elements move from the fluid phase and into the host rocks. This results in mass-gains and losses of the altered host rocks as the system is striving to attain chemical equilibrium (c.f., Susak, 1994). Thus, the alteration assemblages develop the zone refining sequence that is controlled by the temperature, pressure, hydrothermal fluid composition, metal ion concentrations (mass action effect), relative stabilities of soluble complex ions, wall-rock interactions, multiple hydrothermal fluxing and mixing, mineral free energies, and mineral volatilities (c.f., Susak and Crerar, 1982).

Although VMS deposits are less likely to form at very high temperatures, i.e., >350 °C (primarily because high metal solubilities at high temperatures preclude the saturation of metals in hydrothermal fluids), many deposits including Key Anacon occur in metamorphic terranes up to and including amphibolite grade. To recognize these deposits, we need to be able to distinguish those that formed by metamorphic processes from those that were simply metamorphosed. In the case of the latter, we place the emphasis on seeing through the effects of metamorphism (e.g., McFarlane et al., 2007; Marshall and Spry, 2000). Furthermore, because deposits in high-grade metamorphic terranes contain few hydrous phases, identifying pre-metamorphic alteration may be the only way to explore for, or more importantly, understand these deposits (e.g., Hodges and Manojlovic, 1993). Spry (2000) demonstrated that the effects of sulfidation and oxidation on country rocks enclosing metamorphosed massive sulfide deposits constitute an exploration guide to ore. Sulfur and oxygen from the sulfide deposit react with the Fe component of ferromagnesian silicates (e.g., garnet, staurolite,

* Corresponding author.
E-mail address: d4ln8@unb.ca (J.D.S. Zulu).

http://dx.doi.org/10.1016/j.gexplo.2016.02.003
0375-6742/

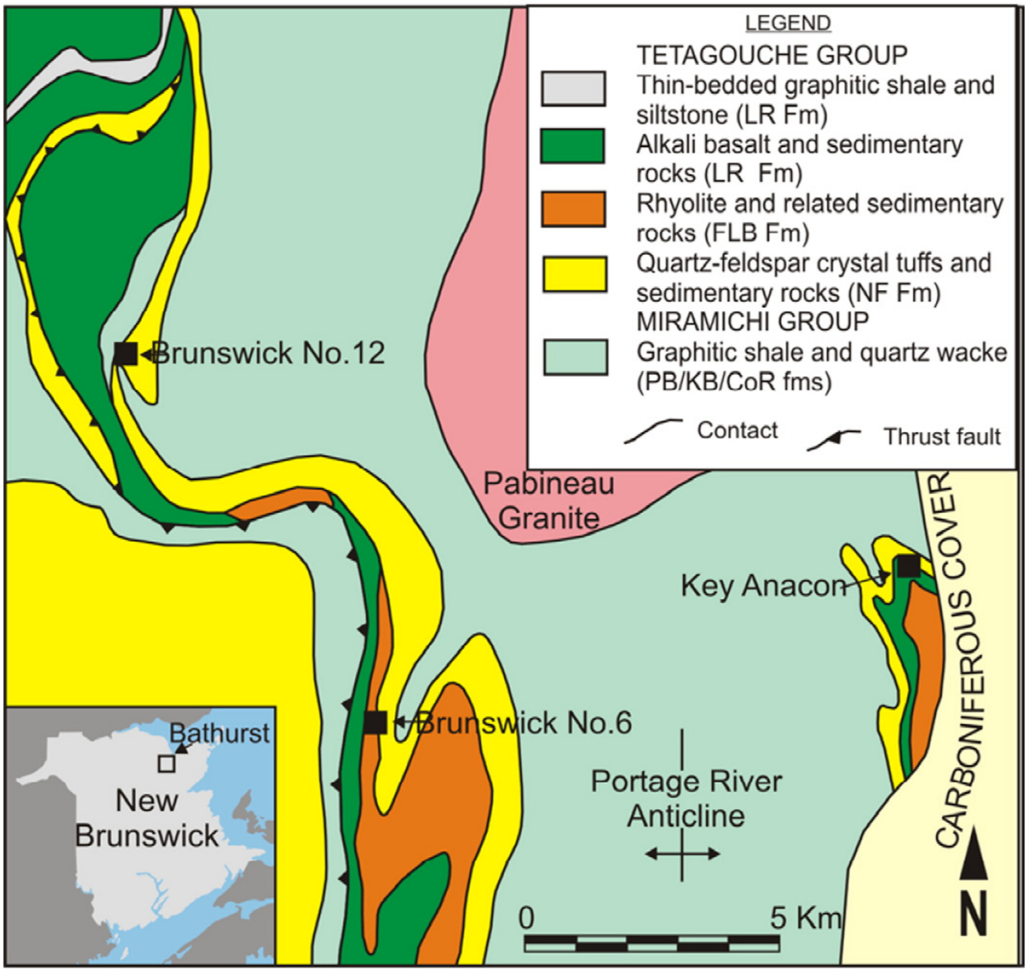

Fig. 1. A Geological map of eastern part of the Bathurst Mining Camp showing location of the Key Anacon,. Brunswick No. 12 and No. 6 deposits, New Brunswick, Canada (modified after van Staal and Williams, 1984). Detailed geology of the Key Anacon deposits is in Fig. 2.

chlorite, and biotite) or oxides (e.g., gahnite and högbomite) to produce Mg- or Zn-rich silicates or Zn-rich oxides with proximity to the ore (Spry and Scott, 1986; Spry, 2000). This halo of Mg-rich or Zn-rich minerals can be superimposed onto zones of pre-metamorphic alteration or can be developed around ore deposits where signs of alteration are apparently absent (Spry, 2000). The compositions of the resulting ferromagnesian silicates and Zn-rich minerals, as well as the distribution end-members of the system Ca–Ti–Fe–S–O, are dictated by the bulk-rock composition and by a variety of physicochemical conditions including T, P, fS_2, fO_2, and fH_2O. Therefore, sulfidation–oxidation haloes are most prominent where a large $fS_2 - fO_2$ gradient is apparent around an ore deposit. Furthermore, the presence of pyrrhotite, pyrite, and magnetite (high $fS_2 - fO_2$ conditions) in a metamorphosed massive sulfide body that is enveloped by graphite-bearing (low fO_2 conditions) country rocks ensures such a gradient (Spry, 2000). Spry (2000) proposed that the proximity and abundance of graphite, in part, dictate the width of the sulfidation–oxidation halo to the massive sulfide body. Where graphite occurs adjacent to a sulfide body the halo will be narrow; however, if graphite occurs tens to hundreds of meters from sulfide mineralization, the likelihood of a wider halo is increased.

Recognizing and documenting the petrogenesis of alteration halos in metamorphic terrains is complicated by: 1) progressive metamorphic dehydration reactions that transform fine-grained hydrous alteration assemblages into medium-grained anhydrous assemblages; 2) mass-losses and gains that can change the bulk composition of the protolith; 3) sulfidation and oxidation reactions associated with the massive sulfide deposit may impart new diagnostic minerals that are stable under specific conditions, and/or restrict nucleation and growth of other mineral phases; and 4) deformation may attenuate large alteration halos into parallelism with tectonic fabrics thereby obscuring the original geometry of the alteration envelops. Therefore, quantification of the mass changes resulting from pre-metamorphic hydrothermal alteration is dependent on a combined understanding of the original bulk composition of the host rock prior to low temperature fluid–rock interactions, as well as the mineralogical and textural evolution of hydrothermal assemblages during prograde metamorphism.

The purpose of this paper is to characterize the pre-metamorphic chemical signature of the alteration assemblage from the regional metamorphic effects at the Key Anacon Zn–Pb–Cu–Ag deposit, located in the Bathurst Mining Camp, New Brunswick (Fig. 1). This deposit was deformed and metamorphosed to the upper-greenschist to amphibolite facies (400–570 °C, 4.1 ± 0.5 kbar) during the Palaeozoic (Zulu, 2012).

2. Geological setting

The rocks of the Brunswick belt are assigned to two lithostratigraphic groups, the Cambro-Ordovician Miramichi Group and the Middle Ordovician Tetagouche Group (Skinner, 1974). The Miramichi Group is dominated by mature quartzose sedimentary sequence, which becomes progressively finer grained and more graphitic towards the contact with the Tetagouche Group rocks (van Staal and Williams, 1984; Lentz, 1996a). Rice and van Staal (1992) interpreted the graphitic phyllites and quartzose wackes as having been formed on an abyssal slope.

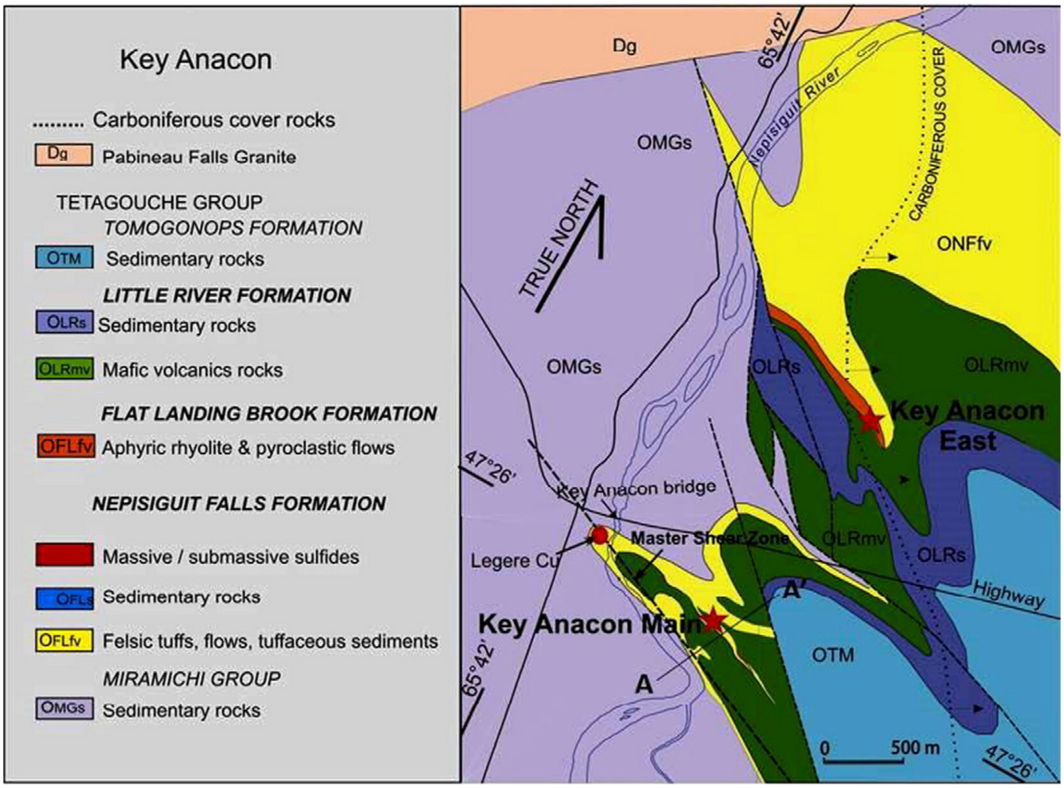

Fig. 2. Geological map showing the location of the Key Anacon Main and Key Anacon East deposits (stars) and the Legere Cu occurrence (red circle), and a section through A–A′, Bathurst Mining Camp. Black dashed-lines are faults. Note: east of the dotted line Cambro-Ordovician rocks are covered by the carboniferous. Area of Figure is outlined on Fig. 1.

The Tetagouche Group disconformably overlies the Miramichi Group and consists of formations that, in ascending stratigraphic order are: Nepisiguit Falls, Flat Landing Brook, Little River, and Tomogonops. The Nepisiguit Falls Formation consists of quartz-feldspar-phyric felsic volcanic and associated sedimentary rocks. This formation has been interpreted as a pyroclastic sequence dominated by crystal-rich ash flow tuffs, reworked tuffites, and related sedimentary (van Staal et al., 1992). Volcanogenic massive sulfide deposits (e.g., Brunswick #12, Brunswick 6, and Key Anacon) and related Algoma-type iron formation occur at the top of the Nepisiguit Falls Formation.

In the eastern part of the Bathurst Mining Camp, the Nepisiguit Falls Formation is overlain by the Flat Landing Brook Formation, which consists of feldspar-phyric to aphyric rhyolite flows, associated breccias and related hyalotuffaceous sedimentary rocks. However, at Key Anacon the Flat Landing Brook Formation is missing and mafic volcanic and related sedimentary rocks of the Little River Formation immediately

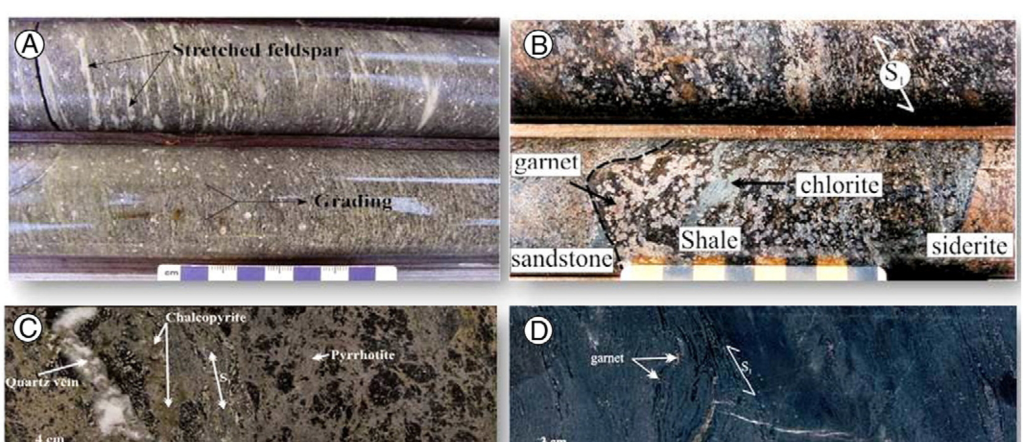

Fig. 3. Photographs of rocks from the Key Anacon deposit A) Nepisiguit Falls Formation felsic crystal tuff with medium-grained feldspar-quartz crystals, drill hole KA92–40 @ 862 m, B) Little River Formation-variably altered mafic volcaniclastic rocks with garnet-biotite ± cordierite porphyroblasts, drill hole KA93-40 @ 578 m. The dark-green color is due to a high content of chlorite in the unit, **C**) syngenetic stockwork vein of chalcopyrite-pyrrhotite-pyrite with a late-stage (post-S_4) quartz vein parallel to S_1 and locally folded in a chlorite-altered felsic tuff (Nepisiguit Falls Formation), drill hole KA92-38 @ 682 m, and D) magnetite-rich sedimentary rocks (Little River Formation) with garnet-biotite porphyroblasts. Sample is from drill hole KA92-42 @ 189.6 m. Note: garnets are concentrated within the phyllosilicate-rich layers. Samples are from the Key Anacon East Zone.

Table 1
Representative whole-rock geochemistry data from the Key Anacon Main Zone deposit.

Felsic volcanic rocks (NF Fm)				Key Anacon Main Zone											
Sample	LPA-71	LPA-72	LPA-73	LPA-74	LPA-76	LPA-77	LPA-82	LPA-83	LPA-86	LPA-95	LPA-99	LPA-106	LPA-107	LPA-118	Avgs
SiO_2	83.20	77.70	74.60	26.80	75.60	69.30	66.40	70.00	62.90	77.60	71.20	62.80	63.40	76.00	68.39
TiO_2	0.21	0.23	0.36	0.58	0.55	0.68	0.58	0.53	0.80	0.65	0.39	0.67	0.72	0.29	0.52
Al_2O_3	7.60	10.80	12.80	9.80	8.00	9.40	13.80	14.10	16.80	10.20	5.60	16.50	16.20	13.00	11.76
Fe_2O_3t	3.80	5.40	4.80	10.20	10.40	14.30	3.70	3.60	7.40	7.10	11.00	5.50	6.10	2.70	6.86
MnO	0.02	0.01	0.05	0.64	0.12	0.22	0.06	0.04	0.05	0.05	0.02	0.14	0.09	0.02	0.11
MgO	0.37	0.55	2.12	9.90	1.44	2.43	1.29	1.12	2.77	0.74	0.33	4.01	3.48	2.38	2.35
CaO	0.52	0.07	0.11	19.70	0.11	0.07	4.12	2.06	2.16	0.12	0.06	3.26	2.40	0.83	2.54
Na_2O	0.10	0.10	0.20	0.20	0.10	0.10	2.80	3.60	2.40	0.20	0.02	2.10	2.10	2.20	1.16
K_2O	1.89	2.85	3.05	0.12	1.68	1.18	2.65	2.06	2.72	2.30	1.27	1.73	1.84	2.30	1.97
P_2O_5	0.03	0.06	0.09	0.16	0.10	0.10	0.13	0.13	0.14	0.10	0.10	0.10	0.13	0.08	0.10
S(t)	2.34	2.88	2.14	4.22	4.38	3.05	0.37	0.24	2.75	1.88	4.76	2.19	3.46	1.07	2.55
Ce	43.00	62.00	84.00	95.00	64.00	74.00	91.00	91.00	130.00	67.00	48.00	120.00	130.0	68.0	83.36
Dy	4.50	6.20	7.10	5.60	4.40	5.40	7.90	8.80	9.90	4.50	3.50	10.00	9.70	7.60	6.79
Er	2.60	3.50	3.70	2.90	2.40	2.90	4.30	4.70	5.00	2.40	1.80	5.60	5.20	4.10	3.65
Eu	0.88	0.94	0.98	1.30	1.70	1.70	1.50	1.20	1.90	1.90	1.60	1.50	1.70	0.58	1.38
Gd	4.40	6.20	7.80	7.30	5.00	6.30	9.30	10.00	13.00	5.60	4.40	12.00	12.00	8.10	7.96
Ho	0.93	1.30	1.50	1.20	0.89	1.00	1.50	1.80	1.90	0.85	0.66	2.00	1.90	1.50	1.35
La	19.00	27.00	37.00	45.00	28.00	36.00	48.00	46.00	64.00	34.00	24.00	59.00	62.00	32.00	40.07
Lu	0.40	0.55	0.57	0.47	0.40	0.53	0.66	0.70	0.79	0.42	0.31	0.85	0.80	0.56	0.57
Nd	20.00	29.00	39.00	43.00	28.00	34.00	45.00	46.00	63.00	31.00	22.00	55.00	59.00	33.00	39.07
Pr	5.10	7.50	10.00	11.00	7.30	9.40	12.00	12.00	17.00	8.60	6.10	15.00	16.00	9.00	10.43
Sm	4.40	6.40	8.20	7.70	5.50	6.70	9.00	9.70	13.00	6.10	4.40	12.00	12.00	7.50	8.04
Tb	0.77	1.10	1.30	1.10	0.81	0.93	1.40	1.50	1.80	0.81	0.62	1.70	1.70	1.30	1.20
Tm	0.44	0.60	0.68	0.50	0.43	0.51	0.68	0.77	0.81	0.41	0.31	0.92	0.83	0.66	0.61
Y	28.00	40.00	43.00	34.00	25.00	30.00	47.00	52.00	55.00	25.00	19.00	60.00	57.00	45.00	40.00
Yb	2.70	3.60	3.80	3.00	2.60	3.30	4.30	4.70	5.10	2.60	1.90	5.70	5.10	4.00	3.74
Ag	2.40	4.10	0.60	6.80	0.50	0.30	0.05	0.10	0.20	0.20	4.80	0.10	0.10	0.05	1.45
Ba	130.00	200.00	280.00	30.00	100.00	90.00	570.00	690.00	730.00	220.00	120.00	270.00	390	470	306.43
Be	1.90	2.10	3.50	5.40	5.40	6.40	5.40	5.10	7.50	6.00	3.60	6.40	6.80	2.80	4.88
Co	2.50	7.00	2.50	2.50	21.00	18.00	5.00	10.00	9.00	9.00	28.00	5.00	5.00	2.50	9.07
Cu	49.00	100.00	30.00	27.00	340.00	120.00	11.00	22.00	16.00	440.00	10,000.00	5.00	5.00	5.00	797.86
Cr	120.00	110.00	74.00	26.00	120.00	74.00	41.00	60.00	70.00	130.00	230.00	130.00	99.00	54.00	95.57
Ni	5.00	40.00	5.00	10.00	20.00	19.00	20.00	40.00	24.00	17.00	16.00	5.00	5.00	5.00	16.50
Sc	6.30	3.90	5.90	7.50	7.40	8.50	10.00	10.00	15.00	9.30	5.70	10.00	10.00	4.00	8.11
Sr	10.00	23.00	10.00	67.00	21.00	10.00	160.00	150.00	210.00	10.00	10.00	220.00	240.0	130.0	90.79
Zn	9600.00	4800.00	110.00	5500.00	46.00	1600.00	39.00	44.00	36.00	14.00	10.00	49.00	52	18	1565.57
V	2.50	2.50	2.50	20.00	36.00	47.00	16.00	12.00	37.00	41.00	19.00	14.00	21.00	2.50	19.50
Cs	1.60	2.60	2.90	0.28	1.40	1.00	4.90	2.30	2.10	2.90	1.80	3.90	2.70	1.80	2.30
Ga	9.80	14.00	17.00	13.00	11.00	12.00	19.00	19.00	23.00	15.00	8.30	22.00	22.00	16.00	15.79
Hf	3.90	4.90	7.00	9.70	10.00	12.00	8.50	8.30	12.00	8.70	6.30	12.00	12.00	5.70	8.64
Mo	1.10	9.80	1.50	1.30	1.80	1.50	0.50	0.20	6.80	0.90	1.60	2.40	2.20	2.00	2.40
Nb	6.30	8.10	11.00	13.00	11.00	14.00	14.00	15.00	19.00	13.00	8.10	18.00	18.00	10.00	12.75
Pb	100.00	100.00	59.00	100.00	18.00	49.00	21.00	23.00	31.00	8.00	7.00	37.00	24.00	11.00	42.00
Rb	77.00	100.00	100.00	4.50	68.00	48.00	100.00	83.00	60.00	100.00	62.00	65.00	67.0	57.0	70.82
Ta	0.70	1.20	1.20	1.20	0.90	1.10	1.00	0.90	1.10	1.30	0.70	1.50	1.30	0.90	1.07
Th	10.00	15.00	18.00	16.00	11.00	13.00	17.00	18.00	24.00	11.00	7.70	24.00	23.00	17.00	16.05
Tl	3.70	4.80	4.60	0.29	11.00	3.80	0.60	0.53	0.72	3.50	0.80	1.20	1.80	0.85	2.73
U	2.50	3.80	4.30	2.30	2.30	3.00	4.10	4.80	4.90	2.80	1.80	5.70	5.10	5.00	3.74
Zr	150.00	190.00	290.00	390.00	450.00	540.00	380.00	330.00	490.00	400.00	300.00	470.00	530.0	220.0	366.43

overlie the massive sulfides and associated iron-formation (van Staal et al., 1992; Lentz and Langton, 1995).

The Little River Formation is overlain by carbonaceous shale and wacke of the Tomogonops Formation, which is differentiated from the Miramichi Group by its locally more calcareous nature and less well developed penetrative fabric.

Five groups of folds are recognized. They can be divided unequivocally on the basis of overprinting, into four generations, but there are no known overprinting relationships between the two youngest groups (van Staal and Williams, 1984).

The thrust-related first deformation D_1 isoclinal (F_1) folds and associated axial planar schistosity (S_1) were progressively deformed into tight-to-isoclinal folds (F_2), resulting into an S_1/S_2 transposition fabric, and are interpreted as high-strain deformation with F_1/F_2 fold interference structure (van Staal and Williams, 1984). D_3 are recumbent and best developed in the western part of the BMC, and D_4 are represented as kink-folds in this area. The earliest folds (F_1A and F_1B) are tight to isoclinal and are related to coeval thrusting resulting from one progressive D_1 event.

3. Deposit stratigraphy

The Key Anacon Main Zone and the Key Anacon East Zone massive sulfide deposits are approximately 15 km east-southeast of the Brunswick No. 12 mine and lies on the eastern limb of the large Portage River Anticline (Figs. 1 and 2). This autochthonous sequence consists of the Miramichi Group (argillite and quartzose-wacke) and the disconformably overlying Tetagouche Group. Here, the Tetagouche Group is divided into four formations that, in ascending stratigraphic order, are: Nepisiguit Falls (felsic volcanic rocks with associated sedimentary rocks), Little River (basalt, siltstone, and shale), and Tomogonops (gray locally calcareous wacke, siltstone and shale).

The Nepisiguit Falls Formation is the immediate footwall to the Key Anacon deposits and consists of and intercalated sequence of sedimentary rocks, ash, fine-grained quartz- and quartz-feldspar crystal tuff and volcaniclastic equivalents (Fig. 3a; Zulu, 2012). Towards the top of the Nepisiguit Falls Formation, enrichment of Zr in the volcanic epiclastic rocks is indicated by $Zr/TiO_2 = 0.13$ as compared to most parts with $Zr/TiO_2 = 0.060$ to 0.098, and is attributed to tectonic imbrication and

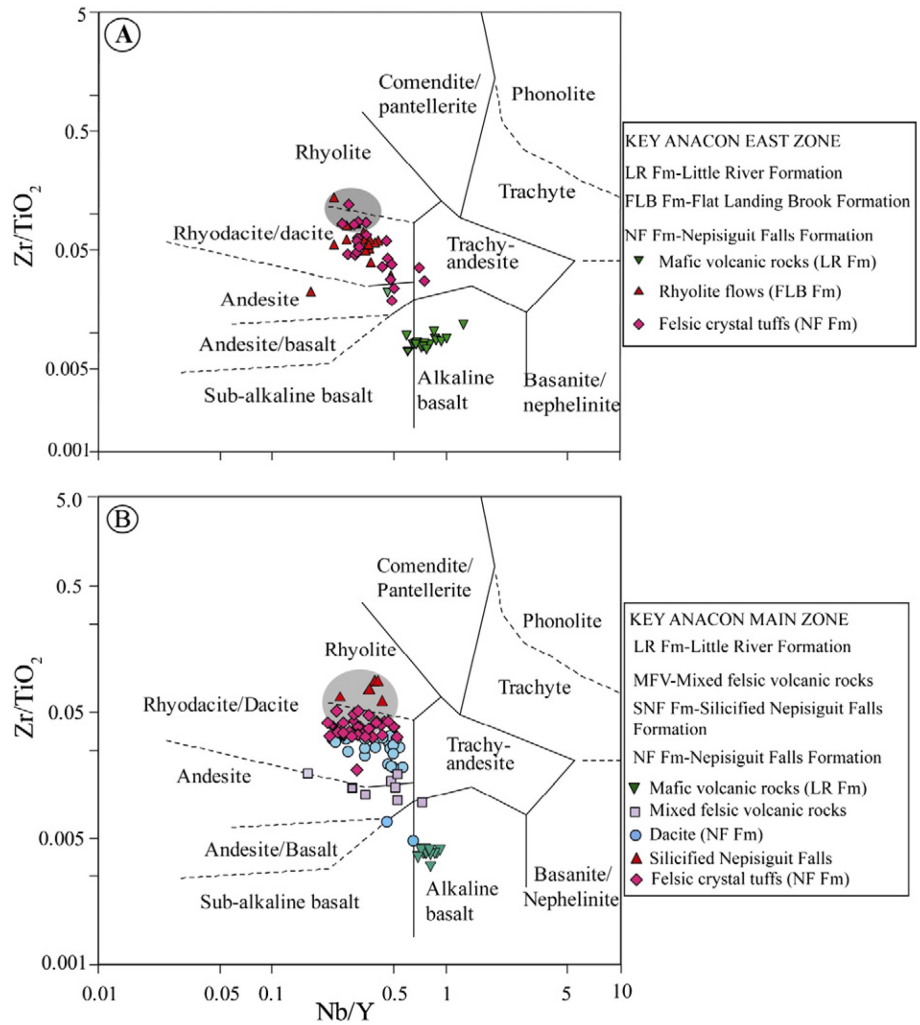

Fig. 4. Zr/TiO_2 versus Nb/Y discrimination diagrams for volcanic rocks. A) Key Anacon East Zone deposit: B) Key Anacon Main Zone. Field boundaries in both diagrams are from Winchester and Floyd (1977).

intercalations of Miramichi Group quartzite(−pelite) with the volcanic rocks in the Nepisiguit Falls Formation.

The Key Anacon Main Zone and East Zone Zn–Pb–Cu–Ag deposits are localized in the hinges of parasitic F_2 folds. Five generations of folds have been recognized in the Key Anacon area (c.f., van Staal and Williams, 1984; Irrinki, 1992; Zulu, 2012). The three earliest phases of folding have an important influence on the large-scale distribution of rocks units (Zulu, 2012). The main geometry of the massive sulfide folds are upright, isoclinal, and steeply plunging sheath-fold structures of the F_2 generation (Zulu, 2012).

4. Methodology

4.1. Lithogeochemical compositions

Under the conditions of hydrothermal alteration, such as those that must have prevailed in the volcanic host rocks (Fig. 3A–D) at the time the Key Anacon deposits formed, the major-elements commonly used for rock type classification (e.g., Si, Na, and K) are highly mobile and consequently, unsuitable for protolith determination. In such cases, robust petrogenetically useful discrimination diagrams, based on elements that are immobile under hydrothermal conditions are used, i.e., the high-field-strength elements (HFSE), which include Al, Ga, Ti, Sc, Zr, Hf, Y, the heavy rare earth elements (HREE) Gd through to Lu, Th, and possibly Nb and Ta (e.g., Floyd and Winchester, 1978; Leitch and Lentz, 1994; Jenner, 1996).

Compiled whole-rock lithogeochemical data of Lentz (1995) and Lentz and Langton (1995) were used to ascertain primary rock types and to document the effects of mineralization-related alteration processes. Fifty-two representative felsic volcanic rock samples (Table 1) were collected from drill cores from the Key Anacon deposit for the purpose of mass-balance calculations, and fifteen ($n = 15$) mafic volcanic rocks for composition discrimination. Major elements analyses were determined by X-ray fluorescence (XRF) spectrometry at four different laboratories (i.e., X-ray Assay laboratories of Don Mills, Ontario; Geological Survey of Canada; ACME Analytical laboratories, Vancouver, BC, and Activation Assay Laboratories, Ancaster, Ontario). The data from all the four laboratories was verified from the QA/QC on standards inserted for each laboratory, and the internal rock standards used are from Lentz (1994). It is important to note that these analyses were done at different times, and the compiled data is in the official New Brunswick Geological Survey Branch lithogeochemical database.

The results of these compiled analyses ($n = 200$) along with analytical methods and detection limits are tabulated in Zulu (2012). Rubidium, Sr, Y, and Zr at XRAL were determined by XRF of pressed powder pellets with a routine precision of 1% for Rb and Sr (2 ppm and 1 ppm detection limits, respectively), 1% for Y (1 ppm detection limit), and 2–3% for Zr (10 ppm detection limit). Rare-earth elements (La, Ce, Pr, Nd, Sm, Eu, Gd, Tb, Dy, Ho, Er, Tm, Yb, and Lu) and trace elements were determined by inductively coupled plasma-mass spectrometry (ICP-MS). Detection limits are of the order of 0.1 ppm for La, Ce, Pr, Nd, Gd, Tb, Dy, Er, Tm, Yb, and Sm, and 0.05 ppm for Eu, Ho, and Lu.

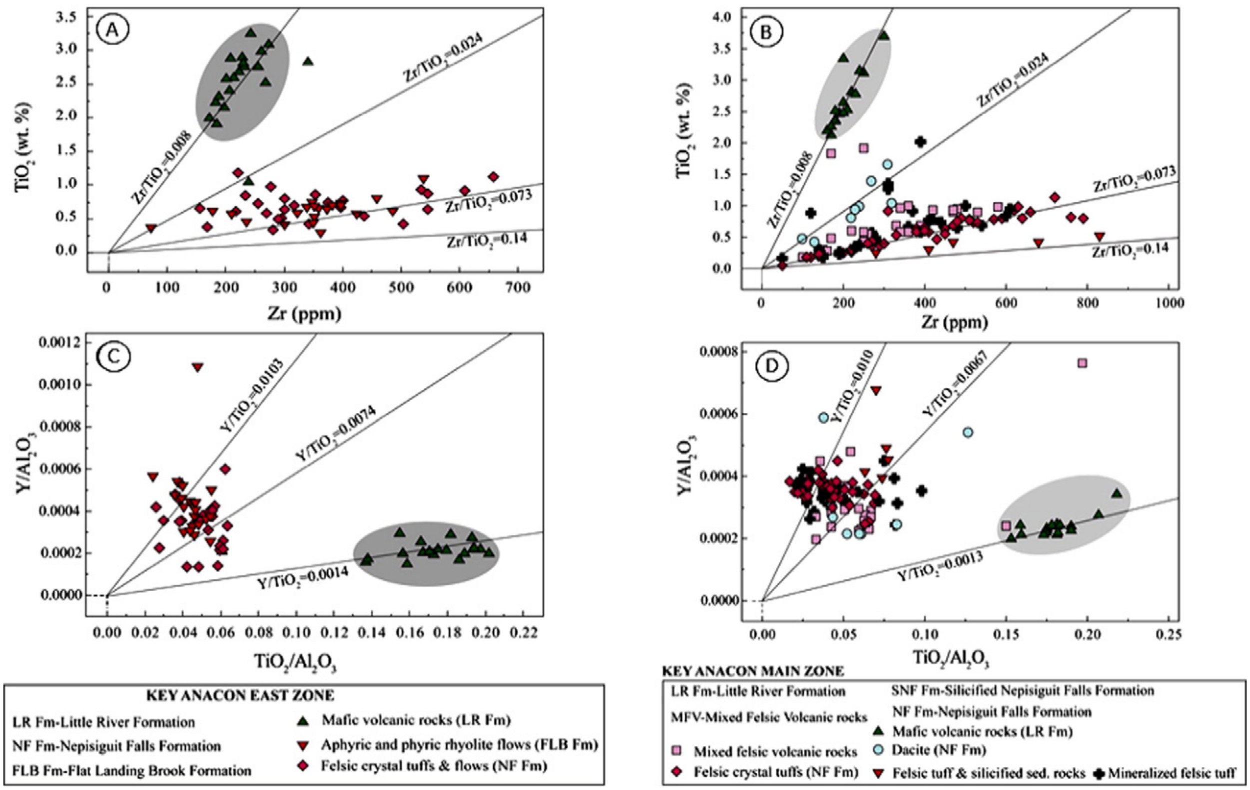

Fig. 5. High field strength element-based differentiation diagrams for volcanic rocks at the Key Anacon East and Key Anacon Main Zone: A and B) Zr versus TiO_2, C and D) TiO_2/Al_2O_3 versus Y/Al_2O_3.

4.2. Thermodynamic modeling of the metamorphosed alteration zone

Altered rock-specific equilibrium assemblage diagrams for the Key Anacon deposits were calculated using the model system K_2O–FeO–MgO–Al_2O_3–SiO_2–H_2O–TiO_2 (KFMASHT), primarily because the major cations present in chloritic and sericitic altered rocks are K^+, Fe^{2+}, Mg^{2+}, Al^{3+}, Si^{4+}, and H^+. In chlorite and sericite altered rocks both CaO and Na_2O tend to be easily mobilized and exert little influence on the overall mineral assemblage (Zulu, 2012). Consequently, modeling a primary alteration system using the system KFMASHT, the metamorphic mineral assemblages developed in hydrothermal altered rocks can be easily predicted using petrogenetic grids and phase diagrams designed for shale or aluminous sedimentary rocks. These grids include thermodynamically calibrated systems, such as K_2O–(FeO or MgO)–Al_2O_3–SiO_2–H_2O (KFASH, KMASH, KFMASH). Thermodynamic calculations were performed using the THERIAK-DOMINO software (de Capitani and Petrakakis, 2010), adopting a gridded Gibbs free-energy minimization approach (Connolly, 2005), and the internally consistent thermodynamic data set of Holland and Powell (1998). The results obtained for two representative samples are presented below.

5. Results

In terms of the Zr/TiO_2 versus Nb/Y discrimination diagram, felsic volcanic rocks assigned to the Nepisiguit Falls Formation in the footwall of both deposits for the most part plot in the rhyodacite/dacite field ($Zr/TiO_2 = 0.060$ to 0.098; Fig. 4), typical for this formation, whereas felsic volcanic rocks in the hanging wall at Key Anacon East Zone (Flat Landing Brook Formation) straddles the boundary between rhyolite and rhyodacite/dacite fields (Fig. 4A). However, some samples ($n = 13$) of feldspar-phyric volcanic and volcaniclastic rocks have more intermediate (andesitic to dacitic) compositions with Zr/TiO_2 ratios of 0.020–0.030 (Fig. 4). There is no known analog in the Nepisiguit Falls Formation for rocks of this composition elsewhere in the Bathurst Mining Camp. Therefore, it is suggested that they be included in a separate member or formation. Most of the mafic volcanic rocks at the Key Anacon East Zone ($n = 15$), plot in the alkaline basalt field and two samples straddle the boundary between sub-alkaline basalt and alkaline basalt fields (Fig. 4A), and, one sample falls within the andesite field. In contrast, all mafic samples from the Key Anacon Main Zone plot in the alkaline basalt field (Fig. 4B).

Based on the Zr/TiO_2 versus Nb/Y classification, two chemostratigraphic units (rhyodacite-dacite and dacite) have been recognized in the footwall rocks (Nepisiguit Falls Formation) at the Key Anacon Main Zone (Fig. 4B). The dacite and the rhyodacite-dacite together occupy the same stratigraphic position as the Nepisiguit Falls Formation (Fig. 4B). The mixed felsic volcanic rocks fall in the andesite field (Fig. 4B), whereas the dacite plots in the rhyodacitic-dacitic field with Zr/TiO_2 ratio that fall below 0.05 (Fig. 4B). Overall, the andesites have immobile trace-element characteristics that are similar to the rhyodacitic rocks of the Nepisiguit Falls Formation, except that their heavy-rare earth elements (HREE) and Y contents are lower (Zulu, 2012).

There are significant chemical differences between the footwall and hanging wall felsic volcanic rocks at the Key Anacon East Zone. Specifically, the higher Zr and lower TiO_2 in the hanging-wall (Flat Landing Brook Formation) relative to the footwall (Fig. 4A and B) reflects increased chemical evolution of the former (Lentz, 1996a). The Nb/Y value of <0.8 is indicative of sub-alkaline composition (Fig. 4A and B), and is consistent with low Zr contents (100–250 ppm) in tuff units (Fig. 5).

The Little River mafic rocks have a dominantly alkali to sub-alkaline basalt signature. The basalts have low Zr/TiO_2 (<0.008) suggesting that Zr is incompatible during fractionation as it strongly partitions into the melt. In contrast, Ti, Cr, Ni, and V are high in the basalts due to presence of olivine, pyroxene, and hornblende (Fig. 5A and B).

The positive correlation between TiO_2 and Zr is also characteristic of alkali basalts, and is interpreted to reflect partial melting and fractionation from more mafic parent composition, as Zr and Ti are both

Table 2
Compositional changes for chemostratigraphic Nepisiguit Falls Formation in the Key Anacon Main Zone deposit.

Sample no	Drill hole	Depth (m)	ΔSiO_2	ΔTiO_2	ΔAl_2O_3	ΔFe_2O_{3t}	ΔMnO	ΔMgO	ΔCaO	ΔNa_2O	ΔK_2O	ΔP_2O_5	ΔS(t)	ΔCe	ΔDy
93-LPA-33	KA92-10	615	−55.67	0.42	0.00	−0.30	0.09	5.54	0.54	−1.92	−2.07	0.00	0.22	63.70	2.78
93-LPA-34	KA92-10	635	−39.68	0.10	0.00	0.10	−0.04	−0.94	−0.27	−1.56	−0.77	−0.05	2.12	33.42	3.48
93-LPA-35	KA92-10	648	−56.69	0.10	0.00	−0.09	0.08	11.80	3.31	−1.96	−3.35	0.03	0.13	29.81	2.48
93-LPA-37	KA92-10	656	−50.09	−0.04	0.00	−0.66	0.34	22.23	26.95	−1.95	−3.78	−0.07	0.52	5.16	2.53
93-LPA-38	KA92-10	662	−46.19	0.01	0.00	1.87	0.41	12.11	33.26	−1.57	−3.45	−0.04	2.99	4.18	4.03
93-LPA-39	KA92-10	664	−44.60	−0.07	0.00	−1.08	0.30	6.69	30.14	−1.04	−3.10	−0.08	1.59	0.40	3.21
93-LPA-41	KA92-10	666	−39.24	−0.05	0.00	3.97	0.50	15.48	49.44	−1.79	−3.53	−0.06	5.51	13.72	3.79
93-LPA-43	KA92-10	681	−29.00	0.18	0.00	3.66	0.08	0.49	0.48	−1.45	−1.11	−0.06	3.70	31.30	2.18
93-LPA-51	KA92-10	755	−38.82	0.10	0.00	0.04	−0.04	−0.96	−0.26	−1.57	−0.68	−0.06	2.10	32.05	3.94
93-LPA-52	KA92-10	804	−51.66	−0.05	0.00	−0.27	0.73	17.43	55.22	−1.94	−3.77	−0.05	0.12	8.79	2.26
93-LPA-54	KA92-10	939	−55.83	0.21	0.00	1.57	0.24	11.69	19.31	−1.96	−3.33	0.11	1.11	23.69	4.17
93-LPA-58	KA93-10	1255	−25.06	0.33	0.00	−0.94	−0.03	1.03	1.65	−0.23	−1.96	0.00	0.36	47.60	2.87
93-LPA-61	KA93-10	1312	−34.18	0.27	0.00	−0.74	−0.01	0.70	0.62	−1.19	−0.32	−0.07	0.00	51.86	2.50

Sample no	Drill hole	Depth (m)	ΔEr	ΔEu	ΔGd	ΔHo	ΔLa	ΔLu	ΔNd	ΔPr	ΔSm	ΔTb)	ΔTm	ΔY	ΔYb
93-LPA-33	KA92–10	615	1.24	0.39	4.02	0.63	31.80	0.42	28.85	7.78	4.70	0.45	0.27	0.86	−38.02
93-LPA-34	KA92–10	635	1.95	0.33	3.90	0.88	11.41	0.47	15.77	4.60	3.66	0.55	0.37	6.49	−37.35
93-LPA-35	KA92–10	648	1.58	0.12	2.33	0.69	8.88	0.49	11.50	3.10	2.10	0.35	0.33	1.06	−37.59
93-LPA-37	KA92–10	656	1.26	−0.21	1.78	0.65	−1.27	0.37	0.76	0.70	0.96	0.39	0.24	−0.13	−38.20
93-LPA-38	KA92–10	662	1.81	0.35	2.88	0.98	−1.26	0.38	0.77	0.66	1.27	0.60	0.30	9.56	−37.90
93-LPA-39	KA92–10	664	1.75	0.32	1.88	0.76	−3.92	0.42	−0.72	0.24	0.59	0.43	0.32	6.84	−37.84
93-LPA-41	KA92–10	666	2.23	0.54	3.57	1.08	2.39	0.46	6.19	1.88	2.58	0.58	0.36	11.07	−37.48
93-LPA-43	KA92–10	681	0.89	0.68	2.77	0.48	10.37	0.29	12.40	3.54	2.70	0.42	0.17	−4.62	−38.82
93-LPA-51	KA92–10	755	2.06	0.25	3.77	0.92	10.80	0.46	17.44	4.43	4.10	0.65	0.36	8.70	−37.31
93-LPA-52	KA92–10	804	1.18	1.08	2.02	0.59	0.96	0.31	2.99	0.99	1.03	0.39	0.20	2.13	−38.53
93-LPA-54	KA92–10	939	2.53	0.52	3.32	0.98	6.72	0.59	11.52	3.41	2.23	0.63	0.50	14.34	−36.81
93-LPA-58	KA93–10	1255	1.69	0.63	3.63	0.72	23.00	0.42	23.52	5.95	3.57	0.59	0.37	5.67	−38.02
93-LPA-61	KA93–10	1312	1.38	0.35	4.36	0.63	21.96	0.38	23.99	6.07	4.20	0.59	0.32	2.48	−38.27

Sample no	Drill hole	Depth (m)	ΔAg	ΔBa	ΔBe	ΔCo	ΔCu	ΔCr	ΔNi	ΔSc	ΔSr	ΔZn	ΔV	ΔCs	ΔGa
93-LPA-33	KA92–10	615	−0.05	−263.56	4.64	0.49	−5.51	8.92	−5.51	7.46	−21.09	−127.40	5.37	−1.05	3.44
93-LPA-34	KA92–10	635	0.15	124.28	1.29	−1.08	−5.08	11.63	−5.08	6.68	78.52	−206.43	−26.82	−0.57	2.53
93-LPA-35	KA92–10	648	−0.08	−572.57	1.22	−1.01	−5.01	−3.24	−5.01	3.97	−30.26	−126.40	−28.42	−1.99	1.75
93-LPA-37	KA92–10	656	0.05	−701.25	−0.16	−0.83	−1.66	5.84	−1.66	2.23	55.30	−203.79	−31.83	−1.91	2.76
93-LPA-38	KA92–10	662	6.67	−619.79	0.24	−0.69	36.95	14.73	−1.39	2.27	82.21	9267.16	−31.69	−1.17	0.87
93-LPA-39	KA92–10	664	3.87	−438.00	0.62	−1.09	32.70	3.93	−2.19	1.28	136.07	4981.33	−32.09	−0.17	0.12
93-LPA-41	KA92–10	666	10.41	−592.79	−0.50	0.42	18.54	16.61	0.85	1.01	98.60	14,253.92	−30.58	−1.60	1.45
93-LPA-43	KA92–10	681	0.47	892.76	1.90	6.47	149.00	42.06	−4.26	8.46	−2.90	−109.95	−18.55	0.17	0.70
93-LPA-51	KA92–10	755	0.15	112.22	1.22	−1.12	−5.12	11.23	−5.12	6.52	65.23	−205.91	−25.78	−0.65	2.28
93-LPA-52	KA92–10	804	−0.03	−726.54	−0.61	0.24	0.49	5.06	0.49	1.28	204.59	−247.76	−30.76	−2.00	3.67
93-LPA-54	KA92–10	939	0.17	−576.53	2.12	1.54	−3.38	17.17	70.50	5.16	32.19	−183.66	−24.84	−1.27	2.55
93-LPA-58	KA93–10	1255	0.03	−124.00	3.56	2.81	2.59	48.83	−0.43	7.11	93.76	−206.60	−4.73	−1.09	2.40
93-LPA-61	KA93–10	1312	−0.07	33.00	2.82	1.89	−4.73	34.68	−0.15	6.78	10.18	−197.70	4.25	0.99	2.01

Sample no	Drill hole	Depth (m)	ΔHf	ΔMo	ΔNb	ΔPb	ΔRb	ΔTa	ΔTh	ΔTl	ΔU	ΔZr
93-LPA-33	KA92–10	615	8.08	3.38	7.94	−9.51	−77.16	0.57	9.91	1.42	1.17	466.94
93-LPA-34	KA92–10	635	5.05	5.51	3.19	10.54	−68.58	0.04	3.75	9.16	1.95	280.51
93-LPA-35	KA92–10	648	4.69	8.07	5.34	−8.02	−113.84	0.42	4.13	2.46	4.71	201.78
93-LPA-37	KA92–10	656	2.48	5.86	0.43	57.05	−126.37	0.23	1.94	−0.71	1.29	98.11
93-LPA-38	KA92–10	662	2.79	4.19	0.96	118.21	−111.13	0.28	2.52	2.27	2.29	109.86
93-LPA-39	KA92–10	664	1.17	2.80	−1.65	102.30	−95.60	0.03	0.77	4.81	2.15	39.96
93-LPA-41	KA92–10	666	2.02	4.69	−0.15	162.90	−112.32	0.10	1.25	2.59	2.53	84.35
93-LPA-43	KA92–10	681	4.09	0.29	1.46	60.76	−52.24	0.27	4.43	11.19	0.45	207.76
93-LPA-51	KA92–10	755	4.91	5.41	2.98	10.77	−69.39	0.26	2.96	9.60	1.76	256.87
93-LPA-52	KA92–10	804	0.89	6.31	−1.99	48.80	−125.64	−0.10	2.75	−0.53	1.43	56.62
93-LPA-54	KA92–10	939	5.28	32.67	5.55	11.86	−103.91	0.61	4.60	2.65	11.12	234.59
93-LPA-58	KA93–10	1255	5.71	−0.74	3.89	6.43	−83.87	0.35	6.90	−0.29	−0.48	288.11
93-LPA-61	KA93–10	1312	4.28	−1.30	2.39	1.70	−61.58	0.40	8.26	−0.59	−2.02	231.13

incompatible in primitive melts. In contrast, Zr is strongly compatible in felsic melts as the fractionation proceeds from andesites through to rhyolite up to SiO_2 contents of 67 wt.%, whereupon Zr fractionates as zircon. The Y/Al_2O_3–TiO_2/Al_2O_3 plots show distinct populations of the Little River mafic rocks, and the Nepisiguit Falls and Flat Landing Brook felsic rocks (Fig. 5C and D).

The Zr/Al_2O_3 index is used to quantify the degree of alteration, with low values signifying mass loss and, high values for mass gain. The Little River mafic rocks have only minor variation in Al_2O_3 content (12.0–16.4 wt.%), which is compatible with the least-altered samples from the hanging-wall, whereas footwall felsic volcanic rocks have variation in Al_2O_3 content (11.5–22.1 wt.%) suggesting strong alteration during chloritization (Zulu, 2012).

5.1. Host rock compositional changes in the Key Anacon deposits

In the footwall sequence of the Key Anacon Main Zone, deposit-related hydrothermal alteration (dominantly seawater) has resulted in a general mass increase in $Fe_2O_{3\ (Total)}$, MgO, and sulfur total (S^T), and mass loss of the alkali and the rare-earth elements. Contents of base metals (Zn, Pb, and Cu), increase in the footwall (or structural hanging wall as there is a stratigraphic inversion) with proximity to the massive

Table 3
AI_{major}, AI_{trace}, AI, GI, and CCPI for chemostratigraphic Nepisiguit Falls Formation in the Key Anacon Main Zone deposit.

DDH no	Sample no	Depth	AImajor	AItrace	AI	GI	CCPI
KA92-5	93-LPA-03	333.97	0.72	0.08	96.27	0.27	71.37
KA92-5	93-LPA-06	391.35	0.89	0.14	91.21	0.51	88.54
KA92-5	93-LPA-07	396.42	0.67	0.05	83.87	0.21	66.52
KA92-5	93-LPA-08	402.50	0.94	0.45	95.95	0.97	93.94
KA92-5	93-LPA-09	409.67	0.63	0.35	94.25	0.23	63.13
KA92-5	93-LPA-11	431.68	0.99	0.98	63.15	9.82	99.37
KA92-5	93-LPA-12	454.80	0.72	0.79	96.14	0.25	71.76
KA92-5	93-LPA-13	462.80	0.72	0.84	84.73	0.28	71.87
KA92-4	93-LPA-21	363.81	0.68	0.13	60.56	0.26	68.07
KA92-4	93-LPA-22	407.73	0.54	0.13	59.94	0.15	53.50
KA92-10	93-LPA-33	614.61	0.86	0.18	89.10	0.37	85.80
KA92-10	93-LPA-34	635.20	0.58	0.04	85.14	0.15	57.88
KA92-10	93-LPA-35	648.13	0.97	0.38	78.19	1.86	97.36
KA92–10	93-LPA-37	655.99	1.00	0.26	46.15	33.26	99.81
KA92-10	93-LPA-38	661.98	0.96	0.97	28.67	2.05	96.29
KA92-10	93-LPA-39	664.03	0.88	0.91	21.52	0.70	87.22
KA92-10	93-LPA-41	666.07	0.98	0.98	25.35	4.43	98.20
KA92-10	93-LPA-43	680.66	0.75	0.14	75.22	0.26	75.12
KA92-10	93-LPA-51	755.49	0.57	0.05	85.18	0.15	56.82
KA92-10	93-LPA-52	803.83	1.00	0.04	25.15	28.18	99.70
KA92-10	93-LPA-54	938.51	0.97	0.21	40.41	2.45	97.44
KA93-10	93-LPA-58	1254.50	0.61	0.06	51.71	0.18	61.27
KA93-10	93-LPA-61	1311.50	0.57	0.06	74.55	0.14	56.44
KA92-17	93-LPA-63	261.20	0.91	0.61	92.45	0.86	91.01
KA92-17	93-LPA-71	491.87	0.68	0.98	78.47	0.31	67.69
KA92-17	93-LPA-72	495.87	0.67	0.94	95.24	0.26	66.85
KA92-17	93-LPA-73	511.87	0.68	0.26	94.34	0.26	68.04
KA92-17	93-LPA-74	523.73	0.98	0.98	33.49	4.07	98.43
KA92-17	93-LPA-76	587.38	0.87	0.67	93.69	0.60	86.93
KA92-17	93-LPA-77	592.13	0.93	0.92	95.50	0.96	92.89
KA92–19	93-LPA-82	189.35	0.48	0.06	36.28	0.13	47.80
KA92-19	93-LPA-83	204.00	0.46	0.07	35.97	0.12	45.47
KA92-23	93-LPA-86	181.16	0.67	0.05	54.63	0.20	66.51
KA92-25	93-LPA-95	59.50	0.76	0.58	90.48	0.36	75.82
KA92-25	93-LPA-99	165.74	0.90	0.98	95.52	0.82	89.81
KA92-26	93-LPA-106	186.50	0.72	0.09	51.71	0.26	71.29
KA92-26	93-LPA-107	191.50	0.71	0.08	54.18	0.25	70.86
KA92-26	93-LPA-118	706.76	0.53	0.03	60.70	0.16	53.03
KA92-26	93-LPA-119	773.35	0.65	0.05	42.93	0.18	65.18
KA92-26	93-LPA-121	805.35	0.73	0.06	65.25	0.24	72.78
KA93-32	93-LPA-131	998.50	0.68	0.05	80.53	0.25	67.77
KA93-32	93-LPA-132	1006.36	0.69	0.31	78.86	0.17	68.55
KA93-32	93-LPA-133	1009.43	0.77	0.02	77.95	0.22	76.49
KA93-32	93-LPA-134	1010.41	0.79	0.07	74.63	0.26	79.30
KA92-2	93-LPA-153	680.20	0.76	0.20	87.21	0.28	75.91
KA92-2	93-LPA-155	862.00	0.91	0.26	57.86	0.73	91.21
KA92-2	93-LPA-156	866.65	0.88	0.46	57.14	0.64	88.32
KA92-2	93-LPA-157	875.00	0.86	0.86	60.11	0.33	85.65
KA92-2	93-LPA-159	939.50	0.90	0.22	48.95	0.57	89.90
KA92-2	93-LPA-163	1000.50	1.00	0.94	89.69	8.02	99.50
KA92-2	93-LPA-165	1041.61	0.95	0.94	74.02	1.43	95.48
KA92-18	93-LPA-167	52.73	0.55	0.06	54.96	0.14	54.35

sulfide lens. The halos defined by the various mass changes extend into the footwall at least 130 m below the massive sulfide lens.

5.2. Compositional change

In order to quantitatively assess the effects of hydrothermal alteration, compositional change calculations were performed using the methodology of Barrett and MacLean (1994), and is as follows:

1. The calculation of an enrichment factor (EF), which is the ratio of Al_2O_3 content in the least-altered sample (precursor) to that of altered sample ($EF = Al_2O_3\ _{(precursor)}/Al_2O_3\ _{(sample)}$. The least-altered composition used for calculations is that of the average Nepisiguit Falls Formation rhyodacite (Langton and McCutcheon, 1993).
2. The reconstructed composition (RC) for each altered sample is determined by multiplying the concentration (wt.% or ppm) of the elements by the correction factor CF (i.e., RC = EF* the concentration of major and trace elements in wt.% and ppm, respectively).

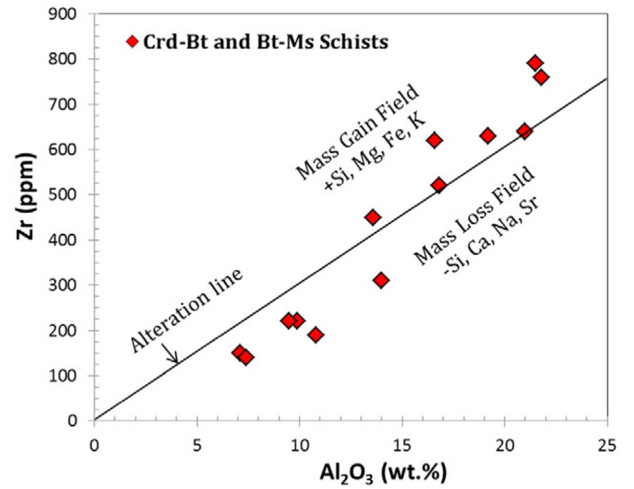

Fig. 6. Zr versus Al_2O_3 plot of metamorphosed altered rocks from the Key Anacon Main Zone. The line represents primary composition; samples above the line have undergone mass gain, whereas samples falling below the line have undergone mass loss. Samples are felsic volcanic rocks from drill hole KA92-10.

Therefore, the compositional change or mass change (MC) for each chemical component is calculated by use of Eq. (1):

$$MC_i = RC_i - PC_i \tag{1}$$

Table 4
Electron Probe Microanalysis of garnet porphyroblast in samples from the Key Anacon East Zone Drill-hole BR94-11.

Rock unit	MG					
Sample no.	BR11–670 m					
Analysis	Core	Annulus 1	Annulus 2	Annulus 3	Annulus 4	Rim
SiO_2	35.66	36.09	35.86	36.08	35.67	36.02
Al_2O_3	20.11	20.22	20.30	20.31	20.28	20.26
TiO_2	0.11	0.15	0.07	0.09	0.07	0.05
Cr_2O_3	0.00	0.00	0.00	0.00	0.00	0.00
Sc_2O_3	0.03	0.09	0.02	0.04	0.01	0.01
Y_2O_3	0.98	0.00	0.00	0.00	0.00	0.00
FeO	16.52	19.96	28.05	33.56	38.66	38.90
MnO	20.38	16.74	12.18	7.24	3.16	2.98
MgO	0.38	0.33	0.72	1.16	1.52	1.38
CaO	3.95	5.61	2.24	1.56	0.45	0.38
Total	98.1	99.2	99.4	100.0	99.8	100.0
Si	5.95	5.92	5.91	5.91	5.86	5.91
Al	0.05	0.08	0.09	0.09	0.14	0.09
Al	3.91	3.83	3.85	3.83	3.79	3.83
Ti	0.01	0.02	0.01	0.01	0.01	0.01
Cr	0.00	0.00	0.00	0.00	0.00	0.00
Sc	0.01	0.01	0.00	0.01	0.00	0.00
Fe^{3+}	0.02	0.19	0.22	0.24	0.33	0.24
Y	0.09	0.00	0.00	0.00	0.00	0.00
Fe^{2+}	2.28	2.54	3.65	4.36	4.98	5.10
Mn	2.88	2.33	1.70	1.00	0.44	0.41
Mg	0.10	0.08	0.18	0.28	0.37	0.34
Ca	0.71	0.99	0.39	0.27	0.08	0.07
Total	16.0	16.0	16.0	16.0	16.0	16.0
X_{Alm}	38.2	41.5	59.4	70.8	80.2	82.8
X_{Sps}	48.1	37.9	27.7	16.3	7.1	6.7
X_{Prp}	1.6	1.3	2.9	4.6	6.0	5.5
X_{Grs}	11.8	16.1	6.4	4.4	1.3	1.1
Fe/(Fe + Mg)	0.96	0.97	0.95	0.94	0.93	0.94
Mg/(Mg + Fe)	0.040	0.031	0.046	0.061	0.070	0.062

Note: Mole fractions of Almandine (X_{Alm}), spessartine (X_{Sps}), pyrope (X_{Prp}), and grossular (X_{Grs}) are average (n = 3 for the core and annulus, n = 4 for the rims) mole % fractions of garnet porphyroblasts. All analyses are in units of wt.% and the calculated ions in atom percent per formula unit (apfu).

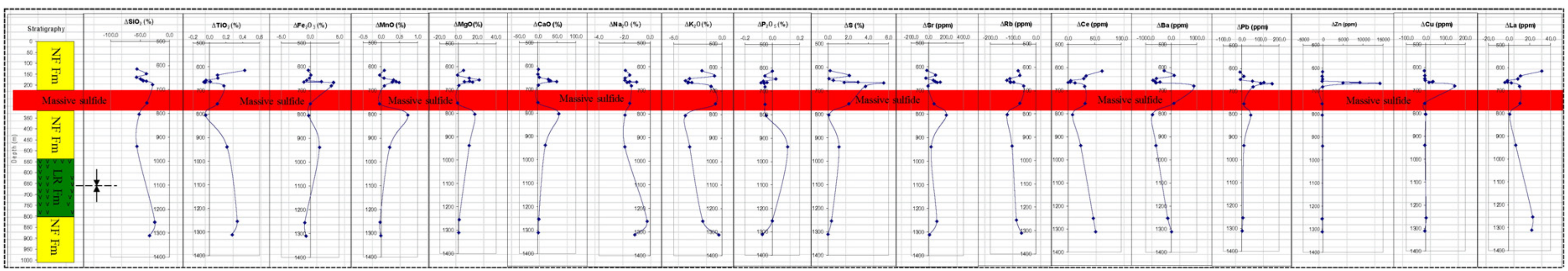

Fig. 7. Down hole variation of major- and trace-element mass changes in drill hole KA92-10. These data illustrates intense footwall alteration characterized by mass addition of Fe_2O_3 $_{(Total)}$, MgO, Pb, Zn, Cu, and S^T, and mass loss of SiO_2, Na_2O, and K_2O relative to the precursor. The hanging wall Nepisiguit Falls Formation rocks have had addition of MnO, Sr, and CaO, and depletion of Na_2O, Rb, and SiO_2. Note that the overall structure is an overturned syncline with fold axis indicated.

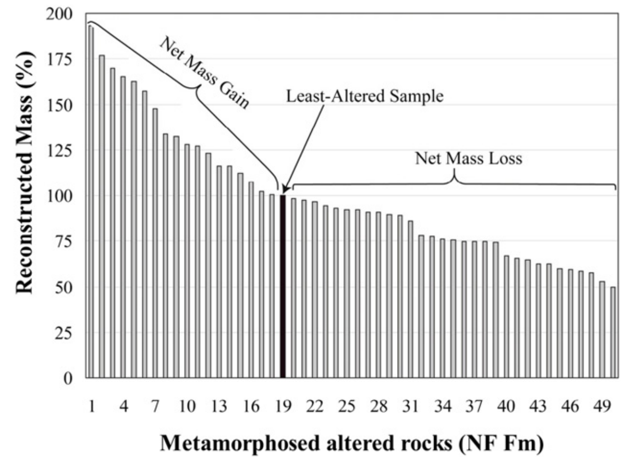

Fig. 9. A histogram of reconstructed mass for the metamorphosed hydrothermal altered felsic volcanic rocks (n = 52) from the NF Fm of the Key Anacon Main Zone. The least altered sample (19) is from drill hole KA92-5 @ 432.18 m.

where MC_i = compositional change (i), RC_i = concentration of element (i) in the reconstructed composition, and PC_i = concentration of element (i) in the least altered sample (i.e., the precursor).

Down hole plots of the mass change for selected element along drill core KA92-10 shows systematic variations in chemical components with respect to the footwall stratigraphy (Fig. 7). Proximal footwall rocks (Nepisiguit Falls Formation) show minor mass loss of K_2O and Na_2O and major mass loss of SiO_2 (Fig. 7). Distal to the massive sulfide lens in the hanging wall, mass change diminishes to the expected values of the unaltered rhyodacite. Furthermore, a drastic reduction in MgO is observed as the massive sulfide lens is approached from both the hanging wall and footwall. Similarly, CaO, MnO, and Sr contents decrease towards the massive sulfide lens from both hanging wall and footwall (Fig. 7).

The calculated compositional changes in major-element oxides for 13 samples from the Nepisiguit Falls Formation at the Key Anacon Main zone along section A–A′, located on Fig. 2, (see also DDH KA92-10; Fig. 8), are listed in Table 2. The compositional variation in the Nepisiguit Falls Formation of the stratigraphic footwall (structural hanging wall) is characterized by overall addition of $Fe_2O_{3(Total)}$, MgO, and S^T, and loss of SiO_2, Na_2O, and K_2O (Fig. 7). These rocks have undergone mass gains of 0.1 to 4.0 wt.% $Fe_2O_{3\ (Total)}$, 0.7 to 22.2 wt.% MgO, and 0.5 to 55.2 wt.% CaO gains, and mass losses of 25.1 to 56.7 wt.% SiO_2, 0.2 to 2.0 wt.% Na_2O, and 0.3 to 3.8 wt.% K_2O. Variable gains and losses of Zn, Pb, and Cu are characteristics of the footwall alteration zones with Zn gains proximal to the sulfide lens, and losses distal to the massive sulfide lens (Fig. 7). The mass changes of Zn range between −248.0 and 14,254.0 ppm, whereas Pb has increased between 1.7 and 162.0 ppm (Table 2). The unit is also characterized by losses of Rb (52.0 to 126.0 ppm) and variable gains or losses in Sr and Ba (Table 2; Zulu, 2012). The net gain in FeO is highest in the core of the alteration zone, whereas the net gain in MgO is highest in the surrounding altered rocks (cordierite–biotite schists; c.f., Franklin, 1997). Some cordierite–biotite bearing rocks have lower chlorite/sericite ratios, reflecting higher abundances of sericite at the margin of the alteration zone.

The mass changes related to hydrothermal alteration in the rocks hosting the Key Anacon deposits can be represented by the binary plots comparing compositional change of major-elements (Fig. 8). Results in Fig. 8 show that chloritization is the dominant alteration type

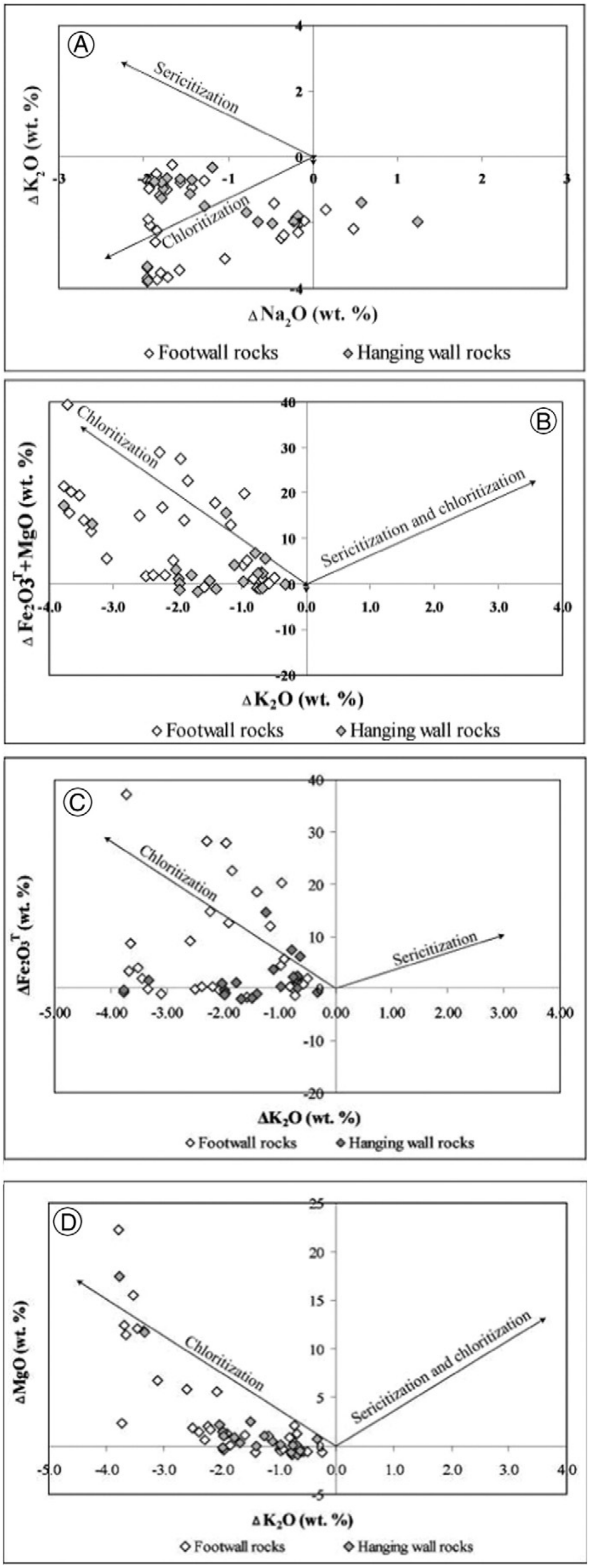

Fig. 8. Binary plots of selected major-element compositional change illustrating the relationships between geochemical variations and alteration mineral assemblage. A) ΔK_2O versus ΔNa_2O, B) $\Delta Fe_2O_{3\ (Total)} + \Delta MgO$ versus ΔK_2O, **C)** $\Delta Fe_2O_{3\ (Total)}$ versus ΔK_2O, and D) ΔMgO versus ΔK_2O (Zulu, 2012). Samples are from the Key Anacon Main Zone in the Nepisiguit Falls Formation.

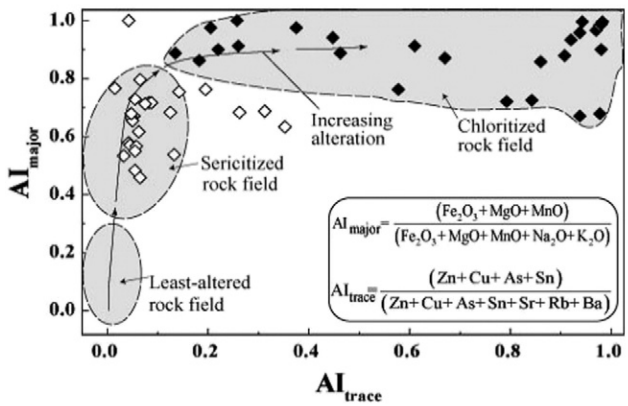

Fig. 10. AI_{major} versus AI_{trace} diagram showing the characteristic fields of the least-altered, sericitized, and chloritized volcanic rocks (Nepisiguit Falls Formation; samples are from the Key Anacon Main Zone (adapted from Häussinger et al., 1993).

affecting the rocks at the Key Anacon Main Zone. Primary chlorite alteration is metamorphosed to biotite and cordierite in the alteration zone. In most drill cores, the metamorphosed alteration halos are symmetrically distributed about the massive sulfide lenses (i.e., footwall and hanging wall alteration; c.f., Wahl, 1977; Lentz, 1995; Lentz and Langton, 1995; Lentz, 1996a). However, asymmetrical alteration halos predominate in zones where sulfide concentration is localized within the F_2 parasitic folds, and is attributed to intense shearing coupled with strain partitioning in altered zones.

The net mass gains and losses in the altered volcanic rocks were calculated, based on the procedure of MacLean and Barrett (1993). The histogram of reconstructed mass changes for both gains and losses related to alteration of the host rocks are illustrated in Fig. 9 and the calculated mass change for major oxides and selected trace elements are presented in Tables 2 and 3. For the purpose of this study, the sample with zero mass change, i.e., the least-altered sample is sample 19 from drill hole KA92–5 @ 432.18 m. (Fig. 9).

5.3. Lithogeochemical alteration indices

Alteration indices (AI) were first proposed by Ishikawa et al. (1976), as a means to quantify the degree of alteration in volcanic rocks hosting the Kuroko-type VMS deposits. These authors proposed the AI ($AI = [(MgO + K_2O)] / [(MgO + Na_2O + K_2O + CaO)]*100$) to assess the degree of sericite and chlorite alteration. This index encompasses reactions involving the breakdown of albite and volcanic glass (Na_2O and CaO loss) and their replacement by sericite and chlorite (K_2O and MgO gain). Typical AI values for unaltered rocks lie between 20 and 60, whereas altered rocks commonly have AI values between 50 and 100, and rocks that have undergone complete replacement by sericite and/or chlorite having $AI = 100$. Häussinger et al. (1993) indicated that any index relating enriched and depleted elements can be equally useful in the estimation of the intensity of alteration; therefore, these authors calculated AI for the major (AI_{major}), and trace (AI_{trace}) elements separately, to improve the recognition of hydrothermal alteration. These AI_{major} versus AI_{trace} diagrams are sensitive to chemical variation related to hydrothermal alteration, and have been effectively employed in this study to document the degree of alteration. The reason for adopting this technique is as follows: during hydrothermal alteration, Fe_2O_3 $_{(Total)}$, MgO, and MnO are added, whereas Na_2O, and K_2O are lost (AI_{major}). Similarly, Zn, Cu, As, and Sn are added, whereas Sr, Ba, and rubidium are lost (AI_{trace}). The two AI equations are:

$$AI_{major} = \left(Fe_2O_3^T + MgO + MnO\right)/\left(Fe_2O_3^T + MgO + MnO + Na_2O + K_2O\right) \quad (2)$$

$$AI_{trace} = (Zn + Cu + As + Sn)/(Zn + Cu + As + Sn + Sr + Ba + Rb). \quad (3)$$

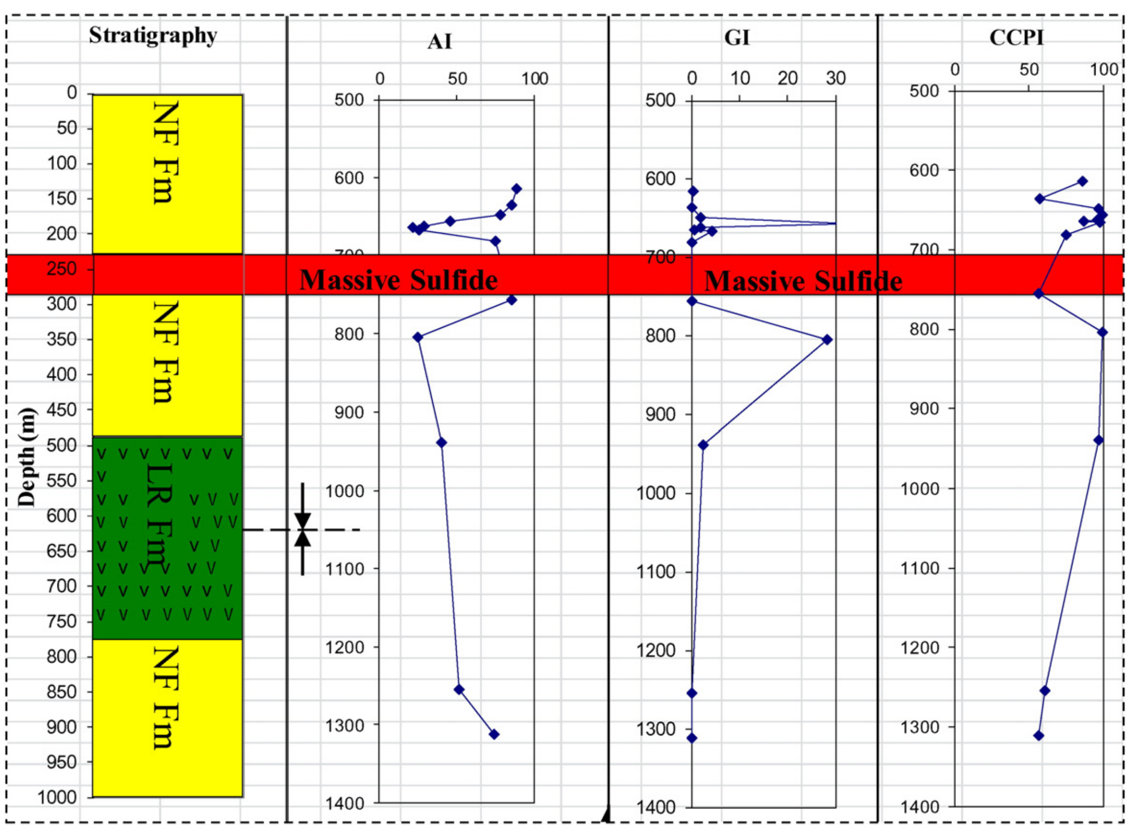

Fig. 11. Down hole plot of AI, GI (in log scale), and CCPI alteration indices for drill hole (KA92-10) at the Key Anacon Main Zone (see Table 3). Note that the overall structure is an overturned syncline with the position of the fold axis indicated (Fig. 12).

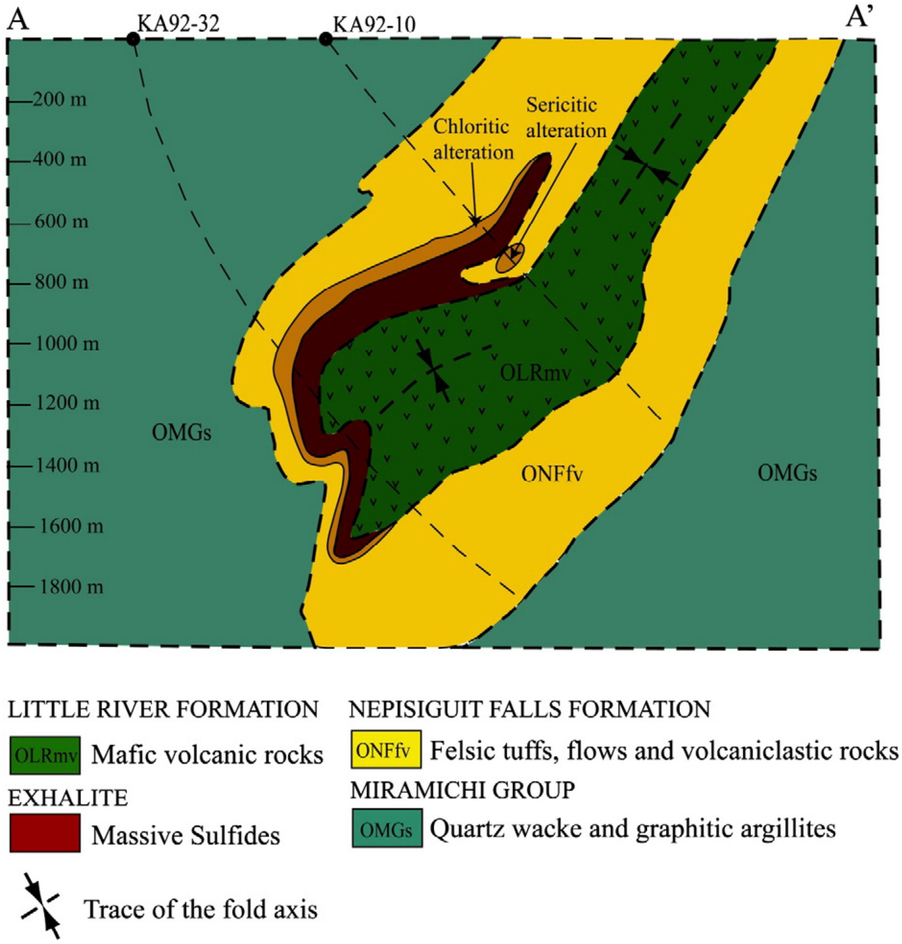

Fig. 12. Geologic cross section through the Key Anacon Main Zone showing position of drill cores KA92-32 and KA92-10. Line of section A–A′ is presented on Fig. 2.

The AI_{major} index generates values between 0 and 1 and is low (<0.24) in the least-altered rocks of the Bathurst Mining Camp (Lentz, 1996b). In contrast, higher values (close to 1) occur in the more intensely chloritized samples (Lentz, 1996b), whereas sericitized rocks have intermediate values (0.5–0.8; Fig. 10). The distinction between the least-altered, and sericitized or chloritized samples is clear and helps to discriminate the degree of alteration of the host rocks; thereby making it an effective and inexpensive vectoring tool. However, these diagrams should be restricted to felsic volcanic host rocks, such as the footwall rocks at the Key Anacon deposits, since mafic host rocks will return higher AI_{major} values, even when unaltered (c.f., Sánchez-España et al., 2000). Contrary to the compositional change evident on binary diagram (Fig. 8), the AI_{major} versus AI_{trace} diagram shows that the rocks in the Key Anacon Main Zone have experienced both chloritic and sericitic alteration (Fig. 10). This is consistent with field observations and thermodynamic modeling of the metamorphosed alteration halo (see below).

The Gandhi index (GI) is another useful alteration index that has been successively employed in describing the type and intensity of chloritization of footwall rocks in the Bathurst Mining Camp (see Lentz, 1996b). The GI is calculated by Eq. (4):

$$\mathrm{GI} = (\mathrm{Fe_2O_{3(total)}} + \mathrm{MgO})/(\mathrm{Na_2O} + \mathrm{K_2O}) \text{ or} \quad (4)$$
$$\mathrm{GI} = (\mathrm{Fe_{(total)}} + \mathrm{Mg})/(\mathrm{Na} + \mathrm{K}).$$

Lentz (1996b) observed that the GI is more robust than the AI since the ratio of the numerators and denominators are divergent (∞/−∞), whereas those of the AI approach unity (0 → 1). In order to resolve the effects of carbonate alteration, Large et al. (2001) derived the Chlorite-Carbonate-Pyrite index (CCPI) that is defined by Eq. (5):

$$\mathrm{CCPI} = [(FeO + MgO)/(FeO + MgO + Na_2O + K_2O) * 100]. \quad (5)$$

Down-hole plots of the AI, GI, and CCPI values for the samples collected from drill core KA92-10 were constructed to test the applicability of these alteration indices to the Key Anacon Main Zone (Figs. 11, 12; Table 3). This drill hole is collared in the stratigraphic footwall (structural hanging wall) and drilled towards the stratigraphic hanging wall and passes through the footwall alteration zone and sulfide lens, mafic rocks of the hanging wall and then down section into the footwall (Fig. 12).

The AI values increase as the massive sulfide lens is approached from either the footwall or hanging wall. In contrast, the GI discriminates the intensely altered chloritic zone, proximal to mineralization in the footwall from the more distal sericitic alteration (Figs. 11 and 12). Overall, there is an increase of the GI values from the weakly to moderately altered zone (GI = 1.30 and 6.04) to the more intensely altered zone (GI = 6.08 and 60; Table 3; Zulu, 2012). Although the down-hole plot of CCPI is similar to that of the GI, it is preferable to adopt the more robust GI, because it is a ratio of the added chemical components ($Fe_2O_{3\,(Total)}$ + MgO) to those lost from the system (Na_2O + K_2O) during the most intense hydrothermal alteration.

5.4. Molar element ratio analysis

Molar element ratio (MER) analysis is a viable alternative to further refine the relationship between alteration-related, major-element

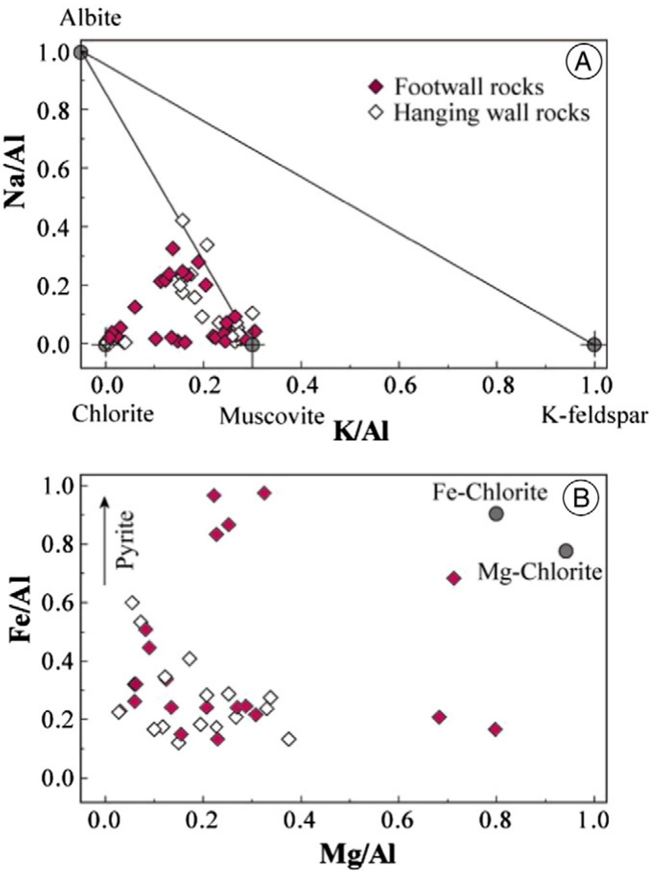

Fig. 13. Molar element ratio plots of 51 samples (Nepisiguit Falls Formation) from the Key Anacon Main Zone stratigraphic hangingwall and footwall. A) Na/Al versus K/Al diagram showing the alteration minerals that control content of Na_2O and K_2O. B) Fe/Al versus Mg/Al discrimination diagram showing variations of Fe_2O_3 $_{(Total)}$ and MgO in the alteration zones. Values of Fe and Mg-rich chlorite in (B) are from microprobe analyses in Appendix E (Zulu, 2012).

lithogeochemical variations, and alteration mineral assemblages (Madiesky and Stanley, 1993). Molar element ratio analysis of data collected from the Nepisiguit Falls Formation rocks in drill hole KA92-10 show the relationship between major-element lithogeochemical variations and the mineral assemblage in the alteration zones. For this purpose, the concentration of Na, K, Mg, and Fe versus Al are effective for displaying mineralogical composition of altered and unaltered rhyolites and rhyodacites plots (Figs. 13 and 14) (e.g., Davies and Whitehead, 2006).

These plots show that chlorite and sericite (or muscovite) are the two main alteration minerals exerting control on the variation of Na_2O and K_2O. The alkali-alumina MER diagram shows a negative correlation between Na/Al and K/Al for sericite-altered rocks, and demonstrates that chlorite is the dominant alteration mineral within the Nepisiguit Falls Formation rocks intersected by drill hole KA92-10 (Fig. 13A). Most samples from the stratigraphic footwall are dominated by chloritic alteration, which is common in highly altered footwall rocks hosting VMS deposits (Lentz, 1996b), whereas the hanging wall rocks are dominated by sericitic alteration (Fig. 13A). The MER discrimination diagrams show that the degree of alteration increases with decreasing Na/Al within the albite-chlorite-muscovite field (i.e., the epidote-chlorite field of Davies and Whitehead, 2006), and is attributed to proximal-type chlorite ± sericite development during feldspar destructive hydrothermal alteration.

In contrast, the Fe/Al versus Mg/Al discrimination diagrams show that the variation in Fe_2O_3 $_{(Total)}$ and MgO is controlled by Fe- or Mg-rich chlorite, and pyrite (Fig. 13B). This diagram reveals that an increase in the Fe/Al of Fe-rich chloritic samples occurs at the expense of low Mg/Al in samples dominated by Mg-rich chlorite.

Similarly, MER plots of Fe/Al versus K/Al, and Mg/Al versus K/Al show that early, low-temperature chlorite alteration in areas distal to the sulfide lens, is overprinted by later intense high-temperature footwall alteration (Fig. 14A). The proximal-type alteration is characterized by Fe-rich chlorite, whereas the distal low-temperature alteration zone is dominated by high Mg-chlorite that locally contains talc and carbonate (Fig. 14B). The distal-type alteration is characterized by feldspar destruction and increasing FeO + MgO to form sericitic alteration zones.

5.5. Metamorphosed alteration zone

It has been demonstrated in this study that two types of deposit-related hydrothermal alteration likely affected the footwall rocks at the Key Anacon deposits, namely: chloritic (+Mg,+Fe,−Ca,−Na,−K), and sericitic (+K,+Mg,±Fe,−Ca,−Na), prior to regional metamorphism. Most samples from the chloritic and sericitic alteration zones have undergone mass loss resulting in apparent enrichment of immobile element contents (Fig. 6). At the upper greenschist- to amphibolites-grade metamorphism reached at Key Anacon, the original hydrothermal alteration facies, i.e., Mg-rich chlorite ± talc ± sericite ± quartz and sericite ± chlorite ± quartz, are characterized by the cordierite–biotite bearing, and garnet-bearing (garnet + chlorite + phengite + biotite + quartz) assemblages, respectively.

The alteration host-rock silicate assemblage around the massive sulfide deposits is commonly overprinted by sulfur-bearing fluids during metamorphism, and is characterized by sulfidation and oxidation reactions (e.g., Spry, 2000). For the Key Anacon deposits, pyrrhotite, pyrite, and magnetite appear to be the reaction products that are produced by destabilization of Fe-Mg-silicates. Two such reactions that may

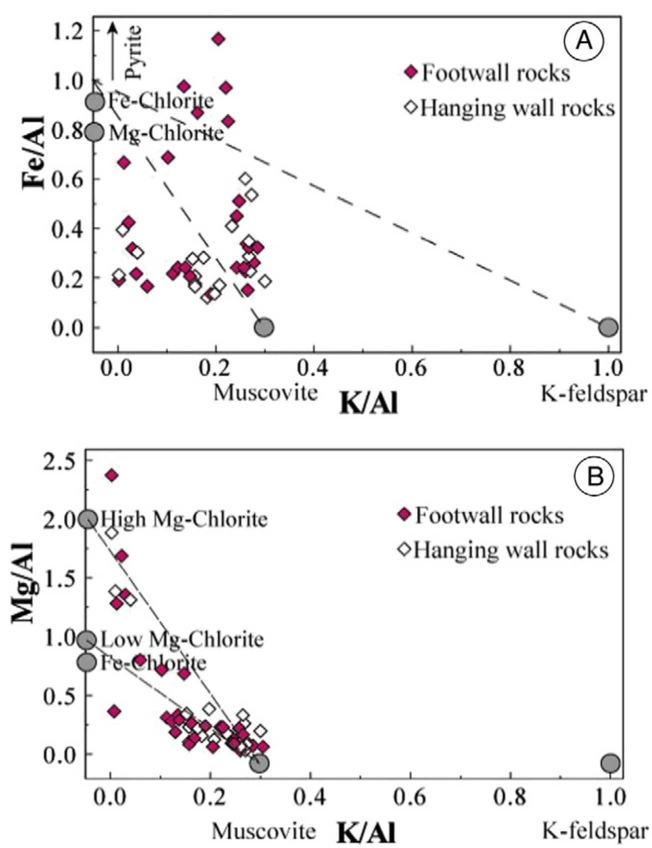

Fig. 14. Molar element ratio plots of 51 samples (NF Fm) from the alteration zones of stratigraphic hanging wall and footwall. A) Fe/Al versus K/Al. B) Mg/Al versus K/Al. The plots illustrates the control of muscovite, Fe-rich chlorite, Mg-rich chlorite, and pyrite on compositional variation of Fe_2O_3 $_{(Total)}$, MgO, and K_2O. Values of Fe and Mg-rich chlorite are from microprobe analyses in Appendix E (Zulu, 2012).

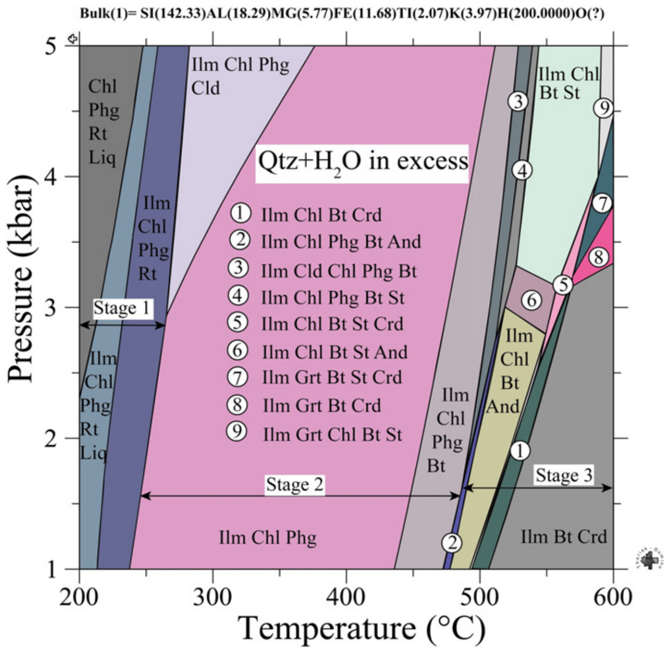

Fig. 15. Petrogenetic grid for altered felsic volcanic rocks (Nepisiguit Falls Formation) showing the modeled *P–T* for a chloritic and minor sericitic alteration. The peak assemblage of sample KA92-10 @ 726 m from the Key Anacon Main Zone is indicated by Ilm + Crd + Bt + Qtz (mineral abbreviations from Whitney and Evans, 2010).

have taken place and involving chlorite and biotite, respectively, are Eqs. (6) and (7):

$$\text{Fe-Mg-rich (Chl)} + S_2 \leftrightarrow \text{Mg-rich (Chl)} + FeS + H_2O \quad (6)$$

$$KFe_3AlSi_3O_{10}(OH)_2 + 1.5S_2 \leftrightarrow KAlSi_3O_8 + 3FeS + H_2O + 1.5O_2. \quad (7)$$

Magnetite is produced during prograde metamorphic conditions when the system has low sulfur fugacity (fS_2) and high oxygen fugacity (fO_2), resulting in reaction (8):

$$KFe_3AlSi_3O_{10}(OH)_2 + 0.5O_2 \leftrightarrow Fe_3O_4 + KAlSi_3O_8 + H_2O. \quad (8)$$

Combining reactions (7) and (8) during sulfidation, yields the important equilibrium relation between magnetite and pyrrhotite, i.e., reaction (9):

$$Fe_3O_4 + 1.5S_2 \leftrightarrow 3FeS + 2O_2. \quad (9)$$

In reactions (6) to (8), the iron component of chlorite and biotite breaks down upon reacting with the vapor phases to form Mg-enriched chlorite and biotite, at the expense of pyrrhotite and magnetite.

Modeling of the chlorite alteration zone in drill core KA92-10 @ 726 m, in the system KFMASHT as a function of pressure (maximum of 4.1 kbar calculated from different barometers) and temperature is shown in Fig. 15. The altered volcanic rocks are metamorphosed to a low-grade mineral assemblage dominated by chlorite, phengite, ilmenite, rutile, and quartz (Stage 1; Fig. 15). These rocks are enriched in Al, Fe, Mg, Ca, and K, and depleted in Si, Ti, and Na suggesting some calcic or sodic hydrothermal alteration. During prograde metamorphism (Stage 2; Fig. 15), chlorite in the chloritic alteration zone breaks down to chlorite and biotite and, subsequently to andalusite at pressures below 3.0 kbar, in both cases forming metamorphic quartz as a product.

The petrogenetic grid for the system KFMASHT indicates that phengite, biotite, and quartz are produced from the breakdown of excess chlorite and sericite at temperatures above 425 °C (stage 2; Fig. 15), consistent with the calibrated system KFMAS of Wang et al. (1986) and Trägårdh (1991). Peak metamorphic assemblage of amphibolite facies conditions for sample KA92-10 @ 720 m, occurs when destabilization of chlorite, phengite, and andalusite results in an assemblage dominated by cordierite + biotite (Crd + Bt) at 3.0 kbar and temperature window of 570–600 °C (stage 3; Fig. 15). This metamorphic assemblage is consistent with petrographic analysis and indicates that a pre-metamorphic K and Mg enrichment attributed to chlorite-sericite alteration proximal to the massive sulfide lenses, affected the footwall rocks.

A well-characterized sample KA92–40 @ 669.2 m (94-DL-87) of sericitic alteration metamorphosed at low grade from the rhyodacite (Nepisiguit Falls Formation), with 0.73 M quantity manganese (Fig. 16), consists mainly of sericite, quartz, and sulfide minerals. These minerals are destabilized during prograde metamorphism (i.e., up to 3.5 kbar and <350 °C) to form chlorite, phengite, microcline, pyrophanite, pyroxmangite, biotite, and quartz (Fig. 16; stage 1). It is interesting that evidence of Mn minerals (pyrophanite and pyroxmangite) is missing in the rocks or in thin sections, but only appear as modeled phases on the petrogenetic grid, suggesting that Mn would occur as minor impurities in other minerals (e.g., chlorite or cordierite) at upper-greenschist facies conditions. At amphibolite facies conditions (on the petrogenetic grid), Mn minerals (pyrophanite and pyroxmangite), microcline, and partly chlorite are consumed in the garnet-forming reaction to form a spessartine-rich garnet core (similar to pelite rocks; Table 4), with the remaining chlorite, phengite, and biotite changing chemical composition (Fig. 16; stage 2). The equilibrium mineral assemblage in sample KA92–40 @ 669.2 m (94-DL-87) is consistent with results predicted from the forward modeling of the metamorphic peak assemblage. These rocks are interpreted to reflect sericitic alteration of felsic volcanic rocks, metamorphosed to the upper greenschist (Fig. 16; stage 2) — amphibolite facies (Fig. 16; stage 3). The mid-upper amphibolite facies conditions represented in shales (e.g., sample BR11–670 m) by an assemblage of *Ilm + Grt ± Phg + Bt + Crd* (mineral abbreviations from Whitney and Evans, 2010) are missing in the altered felsic volcanic rocks, suggesting that peak metamorphic conditions were lower amphibolite facies (see Fig. 16; stage 3). These metamorphic assemblages are interpreted to reflect intense primary metasomatic hydrothermal alteration of felsic host

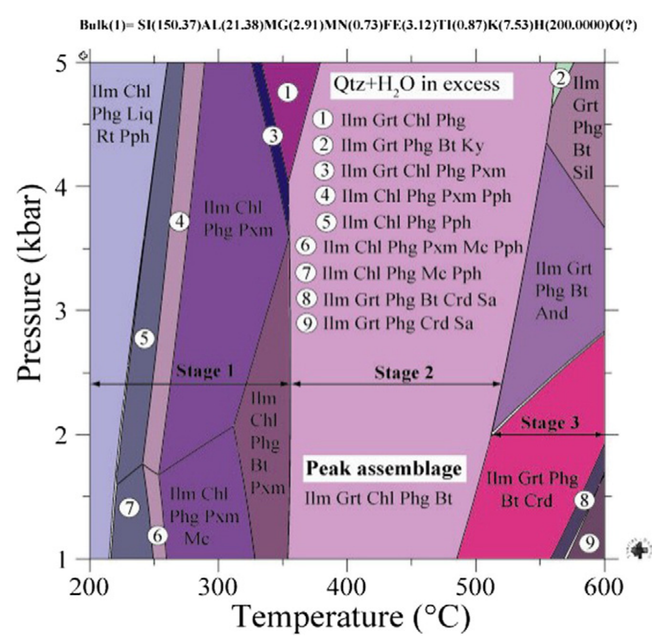

Fig. 16. Petrogenetic grid for altered felsic volcanic rocks (Nepisiguit Falls Formation) showing the modeled pressure–temperature for a sericitic alteration type. The peak assemblage of sample 94-DL-87 from the Key Anacon East Zone is indicated by Ilm = Grt + Chl + Phg + Bt (stage 2) Sample 94-DL-87 (from drill hole KA92–40 @ 669.2 m) comes from the immediate stratigraphic footwall rocks (Nepisiguit Falls Formation) to the massive sulfide deposits (Zulu, 2012). Stages 1 to 3 show progression of metamorphic grade. Mineral abbreviations from Whitney and Evans, 2010).

rocks. Recognition of this primary assemblage is a useful guide in exploring for VMS deposits in medium- to high-grade metamorphic terranes (e.g., Franklin, 1997; Vernon and Clarke, 2008).

6. Discussion and conclusion

In poly-deformed medium- to high-grade metamorphic terranes, well developed hydrothermal alteration zones associated with VMS deposits, such as those along the Brunswick Belt (Lentz, 1999), including the two Key Anacon deposits, can be readily recognized thereby providing important vectors to ore. Metamorphism of hydrothermal alteration zones gives rise to diagnostic, mineral assemblages. For example, the cordierite–biotite (K-bearing) rocks around the massive sulfide deposits, likely formed by metamorphism of a primary Chl $\pm$ Mus $\pm$ Tlc $\pm$ Qtz alteration assemblages. In contrast, the garnet–chlorite–phengite–biotite bearing rocks likely formed by metamorphism of a primary sericite $\pm$ *chlorite* + *quartz* alteration assemblage.

Molar Element Ratio plots of Na/Al versus K/Al, Fe/Al versus K/Al, Mg/Al versus K/Al, and Fe/Al versus Mg/Al (Figs. 13 and 14) demonstrate that the alteration of the volcanic rocks in the Key Anacon deposits were controlled by the formation of sericite (muscovite) and Mg-chlorite from low-temperature hydrothermal fluids, and Fe-chlorite, and pyrite from high-temperature hydrothermal fluids.

The mass changes and down-hole plots of compositional variations are marked by large SiO_2 losses (Table 2; from Zulu, 2012) and systematic variation in the whole rock geochemistry (Fig. 7). Potassium was added to most altered rocks during VMS formation but may have been leached from the cordierite–biotite rock. The alteration zones lost CaO, Na_2O, Ba, Sr, and gained MgO, Fe_2O_3 $_{(Total)}$, MnO, Pb, and Rb (Fig. 7). The net gain in Fe_2O_3 $_{(Total)}$ in footwall rocks was highest in the core of the alteration zone (see Zulu, 2012), whereas the net gain of MgO was highest in areas peripheral to the Fe-rich core (cordierite–biotite rocks).

Down-hole plots of three alteration indices for drill hole KA92-10 at the Key Anacon Main Zone demonstrates that the Gandhi (GI) index is the best vector for identifying mineralization. However, other alteration indices such as the AI are robust and are also useful indices for mineral exploration. The GI index and the Chlorite-Carbonate-Pyrite index (CCPI) are similar (Fig. 11); however the GI index is preferred as it is defined by the ratio of added components (Fe_2O_3 $_{(Total)}$ + MgO) to the leached (Na_2O + K_2O) components.

Acknowledgments

This project is part of a Ph.D thesis to the first author and has been supported by the NB DNR grant to David Lentz and NSERC Discovery grants to both David Lentz and Christopher McFarlane. Dr. Steve McCutcheon is thanked for the discussion about the geology of the Bathurst Mining Camp. We also appreciate thorough analysis and constructive criticism of the two reviewers; Paul G. Spry and David L. Huston who helped us improve the manuscript.

References

Barrett, T.J., MacLean, W.H., 1994. Chemostratigraphy and Hydrothermal Alteration in Exploration for VHMS Deposits in Greenstones and Younger Volcanic Rocks. Geological Association Of Canada, Short Course Notes Vol. 11 pp. 433–467.
de Capitani, C., Petrakakis, K., 2010. The computation of equilibrium assemblage diagrams with Theriak/Domino software. Am. Mineral. 95 (7), 1006–1016.
Connolly, J.A.D., 2005. Computation of phase equilibria by linear programming: a tool for geodynamic modeling and its application to subduction zone decarbonation. Earth Planet. Sci. Lett. 204, 61–74.
Davies, J.F., Whitehead, R.E., 2006. Alkali-alumina and MgO-alumina molar ratios of altered and unaltered rhyolites. Explor. Min. Geol. 15 (1–2), 75–88.
Floyd, P.A., Winchester, J.A., 1978. Identification and discrimination of altered and metamorphosed volcanic rocks using immobile elements. Chem. Geol. 21, 291–306.
Franklin, J.M., 1997. Lithogeochemical and mineralogical methods for base metal and gold exploration. In: Gubins (Ed.), Proceedings of Exploration 97. Fourth Decennial International Conference on Mineral Exploration, pp. 191–208.
Häussinger, H., Okrusch, M., Scheepers, D., 1993. Geochemistry of premetamorphic hydrothermal alteration of metasedimentary rocks associated with the Gorob massive sulphide prospect, Damara Orogen, Namibia. Econ. Geol. 88, 72–90.
Hodges, D.J., Manojlovic, P.M., 1993. Application of lithogeochemistry to exploration for deep VMS deposits in high-grade metamorphic rocks, Snow Lake, Manitoba. J. Geochem. Explor. 48, 201–224.
Holland, T.J.B., Powell, R., 1998. An internally-consistent thermodynamic data set for phases of petrological interest. J. Metamorph. Geol. 16, 309–343.
Irrinki, R.R., 1992. Key Anacon sulfide deposit, Gloucester County, New Brunswick. Explor. Min. Geol. 1, 121–129.
Ishikawa, Y., Sawaguchi, T., Iwaya, S., Horiuchi, M., 1976. Delineation of prospecting targets for Kuroko deposits based on modes of volcanism of underlying dacites and alteration haloes. Min. Geol. 26, 105–117.
Jenner, G.A., 1996. Trace element geochemistry of igneous rocks: geochemical nomenclature and analytical geochemistry. In: Wyman, D.A. (Ed.), Trace Element Geochemistry of Volcanic Rocks: Application for Massive Sulphide Exploration. Geological Association Of Canada, Short Course Notes Vol. 12, pp. 51–78.
Langton, J.P., McCutcheon, S.R., 1993. Brunswick Project, NTS 21 P/5 west, 21 P/4 west, Gloucester County, New Brunswick. In: Abbott, S.A. (Ed.)New Brunswick Department Of Natural Resources And Energy, Mineral Resources, Information Circular Vols. 93-1, pp. 31–51.
Large, R.R., Gemmel, J.B., Paulick, H., 2001. The alteration box plot: a simple approach to understanding the relationship between alteration mineralogy and lithogeochemistry associated with volcanic-hosted massive sulphide deposits. Econ. Geol. 96, 957–971.
Leitch, C.H.B., Lentz, D.R., 1994. The Gresens approach to mass balance constraints of alteration systems: methods, pitfalls, examples. In: Lentz, D.R. (Ed.), Alteration and Alteration Processes Associated With Ore-Forming Systems. Geological Association Of Canada, Short Course Notes Vol. 11, pp. 161–192.
Lentz, D.R., 1994. Preliminary evaluation of six in-house rock geochemical standards from the Bathurst Camp, New Brunswick. In: Merlini, S.A.A. (Ed.), Current Research. Miscellaneous Report Vol. 18, pp. 81–89.
Lentz, D.R., 1995. Stratigraphy and structure of the Key Anacon massive-sulphide deposits compared with the Brunswick deposits, Bathurst Mining Camp, New Brunswick. In: Langton, J.P. (Ed.), New Brunswick Department of Natural Resources and Energy, Minerals and Energy Division, Geoscience Research 1994. Miscellaneous Report Vol. 15, pp. 23–44.
Lentz, D.R., 1996a. Trace-element systematics of felsic volcanic rocks associated with massive-sulphide deposits in the Bathurst Mining Camp: petrogenetic, tectonic and chemostratigraphic implications for VMS exploration. In: Wyman, D.A. (Ed.), Trace Element Geochemistry of Volcanic Rocks: Applications for Massive Sulphide Exploration. Geological Association Of Canada, Short Course Notes Vol. 12, pp. 359–402.
Lentz, D.R., 1996b. Recent advances in lithogeochemical exploration for massive-sulphide deposits in volcano-sedimentary environments: petrogenetic, chemostratigraphic, and alteration aspects with examples from the Bathurst Camp, new Brunswick. In: Carroll, B.M.W. (Ed.), Current Research. New Brunswick Department Of Natural Resources And Energy, Minerals and Energy Division, Mineral Resource Report Vols. 96-1, pp. 73–119.
Lentz, D.R., 1999. Petrology, geochemistry, and oxygen isotope interpretation of felsic volcanic and related rocks hosting the Brunswick No. 6 and No. 12 massive sulfide deposits, Bathurst Mining camp, Canada. Econ. Geol. 94, 57–86.
Lentz, D.R., Langton, J.P., 1995. Key Anacon East Zone Massive Sulphide Deposit: a New Discovery in the Bathurst Mining Camp, New Brunswick. PDA Abstract Volume, Toronto, Ontario ((10) pp.).
MacLean, W.H., Barrett, T.J., 1993. Lithogeochemical techniques using immobile elements. J. Explor. Geochem. 48, 109–133.
Madiesky, H.E., Stanley, C.R., 1993. Lithogeochemical exploration of metasomatic zones associated with volcanic-hosted massive sulfide deposits using Pearce Element Ratio analysis. Int. Geol. Rev. 35, 1121–1148.
Marshall, B., Spry, P.G., 2000. Discriminating between regional metamorphic remobilization and syn-tectonic emplacement in the genesis of massive sulfide ores. Rev. Econ. Geol. 11, 39–79.
McFarlane, C.R.M., Mavrogenes, J.A., Tomkins, A.G., 2007. Recognizing hydrothermal alteration through a granulite facies metamorphic overprint at the challenger Au deposit, South Australia. Chem. Geol. 243, 64–89.
Rice, R.J., van Staal, C.R., 1992. Sedimentological studies in the Ordovician Miramichi, Tetagouche, and Fournier groups in the Bathurst camp and the Belledune-Elmtree Inlier, northern New Brunswick. Current Research, Geological Survey of Canada, Paper 92-1D, pp. 257–264.
Sánchez-España, J., Velasco, F., Yusta, I., 2000. Hydrothermal alteration of felsic volcanic rocks associated with massive sulphide deposition in the northern Iberian Pyrite Belt (SW Spain). Appl. Geochem. 15, 1265–1290.
Skinner, R., 1974. Geology of the Tetagouche Lakes, Bathurst, and Nepisiguit Falls map-areas, New Brunswick with emphasis on the Tetagouche Group. Geol. Surv. Can. Mem. 371 ((133) pp.).
Spry, P.G., 2000. Sulfidation and oxidation haloes as guides in the exploration for metamorphosed massive sulfide ores. Rev. Econ. Geol. 11, 149–161.
Spry, P.G., Scott, S.D., 1986. Zincian spinel and staurolite as guides to ore in the Appalachians and Scandinavian Caledonides. Can. Mineral. 24, 147–163.
van Staal, C.R., Williams, P.F., 1984. Structure, origin and concentration of the Brunswick 12 and 6 orebodies. Econ. Geol. 79, 1669–1692.
van Staal, C.R., Fyffe, L.R., Langton, J.P., McCutcheon, S.R., 1992. The Ordovician Tetagouche Group, Bathurst Camp, northern New Brunswick, Canada: history, tectonic setting, and distribution of massive-sulphide deposits. Explor. Min. Geol. 1, 93–103.
Susak, N.J., 1994. Alteration factors affecting ore deposition. In: Lentz, D.R. (Ed.), Alteration and Alteration Processes Associated with Ore-forming Systems. Geological Association Of Canada, Short Course Notes Vol. 11, pp. 69–99.

Susak, N.J., Crerar, D.A., 1982. Factors controlling mineral zoning in hydrothermal ore deposits. Econ. Geol. 77, 476–482.

Trägårdh, J., 1991. Metamorphism of magnesium-altered felsic volcanic rocks from Berglagen, central Sweden: a transition from Mg-chlorite- to cordierite-rich rocks. Ore Geol. Rev. 6, 485–497.

Vernon, R.H., Clarke, G.L., 2008. Principles of Metamorphic Petrology. Cambridge University Press, New York, U.S.A (446 pp.).

Wahl, J.L., 1977. Rock geochemical exploration at the Heath Steele and Key Anacon deposits, New Brunswick: Unpublished Ph.D. thesis, University of New Brunswick, Fredericton, New Brunswick, (429) pp.

Wang, G.-F., Banno, S., Tackeushi, K., 1986. Reactions to define the biotite isograd in the Ryoke metamorphic belt, Kii Peninsula, Japan. Contrib. Mineral. Petrol. 93, 9–17.

Whitney, D.L., Evans, B.W., 2010. Abbreviations for names of rock-forming minerals. Amer. Mineral. 95, 185–187.

Winchester, J.A., Floyd, P.A., 1977. Geochemical discrimination of different magma series and their differentiation products using immobile elements. Chem. Geol. 20, 325–343.

Zulu, J.D.S., 2012. Deformation and metamorphism of the Key Anacon Zn-Pb-Cu-Ag deposits, Bathurst Mining Camp, New Brunswick, Canada. Unpublished Ph.D. thesis, Fredericton, New Brunswick, University of New Brunswick, (576) pp.